# Dbl3 drives Cdc42 signaling at the apical margin to regulate junction position and apical differentiation

Ceniz Zihni,[1] Peter M.G. Munro,[2] Ahmed Elbediwy,[1] Nicholas H. Keep,[3] Stephen J. Terry,[1] John Harris,[4] Maria S. Balda,[1] and Karl Matter[1]

[1]Department of Cell Biology and [2]Imaging Unit, Institute of Ophthalmology, University College London, London EC1V 9EL, England, UK
[3]Crystallography, Institute for Structural and Molecular Biology, Birkbeck, University of London, London WC1E 7HX, England, UK
[4]Nikon Imaging Centre, King's College London, London SE1 1UL, England, UK

Epithelial cells develop morphologically characteristic apical domains that are bordered by tight junctions, the apical–lateral border. Cdc42 and its effector complex Par6–atypical protein kinase c (aPKC) regulate multiple steps during epithelial differentiation, but the mechanisms that mediate process-specific activation of Cdc42 to drive apical morphogenesis and activate the transition from junction formation to apical differentiation are poorly understood. Using a small interfering RNA screen, we identify Dbl3 as a guanine nucleotide exchange factor that is recruited by ezrin to the apical membrane, that is enriched at a marginal zone apical to tight junctions, and that drives spatially restricted Cdc42 activation, promoting apical differentiation. Dbl3 depletion did not affect junction formation but did affect epithelial morphogenesis and brush border formation. Conversely, expression of active Dbl3 drove process-specific activation of the Par6–aPKC pathway, stimulating the transition from junction formation to apical differentiation and domain expansion, as well as the positioning of tight junctions. Thus, Dbl3 drives Cdc42 signaling at the apical margin to regulate morphogenesis, apical–lateral border positioning, and apical differentiation.

## Introduction

Epithelial differentiation requires the development of a characteristic cell morphology and the establishment of distinct apical and basolateral cell surface domains (Mellman and Nelson, 2008). In vertebrates, these cell surface domains are separated by tight junctions, which form the apical–lateral border. The apical membrane often develops distinctive organ-specific and functionally important morphological adaptations, such as brush border membranes in simple columnar epithelia or the phagocytic apical membrane of retinal pigment epithelia. Although the position of tight junctions defines the relative sizes of the apical and basolateral membranes, the processes that regulate the absolute size of these domains are still poorly understood.

Cell surface polarization relies on counteracting regulators that specify apical and basolateral identity, such as the apical factors Cdc42, ezrin, and atypical PKC (aPKC) and the pro-basolateral scribble complex (Goldstein and Macara, 2007; Yamanaka and Ohno, 2008; St Johnston and Sanson, 2011). The activities of these counteracting mechanisms determine the positioning of the junctional complex and the relative sizes of the apical and basolateral cell surface domains. In *Drosophila melanogaster*, apical factors are concentrated in the marginal zone, a domain just apical to adherens junctions, the apical–lateral border in insects; in vertebrates, the analogous apical signaling zone is thought to be the tight junction, as a marginal zone-like structure has not been described (Pieczynski and Margolis, 2011; Tepass, 2012).

The small GTPase Cdc42 drives apical differentiation by stimulating aPKC via the interacting adaptors Par6 and Par3 (Hall, 2005; Bryant and Mostov, 2008). In epithelia, the

M.S. Balda and K. Matter contributed equally to this paper.

Correspondence to Karl Matter: k.matter@ucl.ac.uk; or Maria S. Balda: m.balda@ucl.ac.uk

S.J. Terry's present address is Randall Division of Cell and Molecular Biophysics, King's College London, London SE1 1UL, UK.

Abbreviations used in this paper: aPKC, atypical PKC; DPPIV, dipeptidyl peptidase IV; FRET, fluorescence resonance energy transfer; GEF, guanine nucleotide exchange factor; GAP, GTPase activating protein.



The Rockefeller University Press $30.00
J. Cell Biol. Vol. 204 No. 1 111–127
www.jcb.org/cgi/doi/10.1083/jcb.201304064

Par3–Par6–aPKC complex has two sequential functions: first, it stimulates junction formation and, second, it regulates apical domain differentiation and positioning of the apical–lateral border (Suzuki and Ohno, 2006; Morais-de-Sá et al., 2010; Walther and Pichaud, 2010). The second function is based on the transitory, dynamic nature of the Par3–Par6–aPKC complex, as Cdc42-stimulated phosphorylation of Par3 by aPKC leads to destabilization of the complex and segregation of Par6–aPKC into the expanding apical domain and retention of Par3 at the apical–lateral border. Despite the well-established importance of this pathway in epithelial differentiation, how this transition is stimulated and how the Par6–aPKC complex is activated in a process-specific manner to drive apical differentiation is not understood.

Another unresolved question is how Cdc42 itself is regulated to drive apical domain differentiation. Rho GTPases are activated by guanine nucleotide exchange factors (GEFs) and inactivated by GTPase activating proteins (GAPs), which are thought to be critical for their spatial and temporal regulation (Hall, 2005). Cdc42 GEFs and GAPs that regulate junction formation, membrane trafficking, and mitotic spindle orientation have been identified (Liu et al., 2004; Otani et al., 2006; Wells et al., 2006; Bryant et al., 2010; Qin et al., 2010; Elbediwy et al., 2012). However, how Cdc42 is activated at the developing apical membrane once junctions have been established to stimulate apical membrane differentiation and junctional positioning is not known.

Here, we describe the identification of Dbl3, a previously uncharacterized isoform of Dbl/MCF2, that is recruited to the apical membrane and becomes enriched at a marginal zone apical to tight junctions. Dbl3 activates apical Cdc42 signaling to drive the Par6–aPKC pathway toward apical differentiation and brush border membrane induction, thereby regulating expansion and size of the apical domain and positioning of the apical–lateral border.

## Results

### Dbl/MCF2 is required for morphogenesis and apical membrane differentiation

We performed an siRNA screen to identify Rho GTPase GEFs important for epithelial differentiation using the human intestinal epithelial cell line Caco-2, which forms polarized monolayers with a differentiated apical brush border membrane. Cell polarization and junction assembly was monitored by staining for the polarity markers dipeptidyl peptidase IV (DPPIV) and $Na^+/K^+$-ATPase, and the junctional markers ZO-1 and α-catenin (Elbediwy et al., 2012). Several GEFs were identified, which included components that had previously been linked to epithelial junction formation and stability such as ECT2 and Trio (Liu et al., 2004; Yano et al., 2011; Ratheesh et al., 2012; Fig. S1 A).

Targeting the GEF Dbl/MCF2 revealed a distinct phenotype, as the cells formed continuous junctions but remained flat and failed to accumulate DPPIV at the apical membrane (Fig. 1 A and Fig. S1, B–D). The cells also did not form the typical apical actin cytoskeleton indicative of brush border membranes, suggesting that depletion of Dbl disrupted apical differentiation. Transepithelial electrical resistance and tracer diffusion assays indicated that Caco-2 cells with reduced Dbl expression still formed functional diffusion barriers in agreement with the continuous junctional distribution of ZO-1 (Fig. S1, E–G). As Dbl depletion resulted in less compacted cells with an increased planar area, the junctions were more stretched (Fig. S1, E and H).

Dbl is a GEF for Cdc42 (Hart et al., 1991). Depletion of Dbl indeed led to an ∼50% reduction in active Cdc42 (Fig. S1 J). RhoA and Rac1 activities were not affected. Although Dbl can stimulate RhoA, its apparent preference for Cdc42 had also been observed during cell migration (Snyder et al., 2002; Prag et al., 2007).

Aside from the unexpectedly high apparent molecular mass of Dbl in Caco-2 cells of ∼140 kD as opposed to the commonly studied variants with a lower molecular mass (Fig. S1 D), it was surprising that it promoted epithelial differentiation rather than cell flattening and migration, as described for other cell types (Prag et al., 2007). However, differentially spliced Dbl isoforms had been identified but their functions had not been analyzed (Fig. 1 A). The Dbl antibody we generated was raised against a peptide contained within a region common to all isoforms C-terminal to the Cral-Trio domain. A larger splice variant, Dbl3, is expressed in various tissues including the intestine; however, its function and localization are not known (Komai et al., 2002, 2003). By RT-PCR, the mRNA transcript for this high molecular mass Dbl isoform was also detected in Caco-2 cells along with shorter variants (Fig. 1 B). On the protein level, the lower molecular mass isoforms were not evident, possibly because of the short half-life of at least some Dbl isoforms (Fig. S1 D; Kamynina et al., 2007). Transfected myc-tagged Dbl3 ran with an apparent molecular mass of ∼140 kD, whereas the more commonly studied Dbl1 isoform exhibited a lower molecular mass of 130 kD (Fig. S2 A). In contrast to the shorter isoforms, Dbl3 contains a complete Cral-Trio domain at its N terminus (Fig. 1 A). Structural modeling predicted that only the Cral-Trio domain of Dbl3 is able to form a stable domain structure, whereas the truncated N-terminal domains of the other isoforms are unlikely to fold into stable domains, possibly underlying their apparent instability (Fig. 1 C). Given that only Dbl3 contains an intact Cral-Trio domain, it seems that this isoform is the more ancient form of the protein.

To determine the role of Dbl3, we designed siRNAs targeting its distinct N terminus. These siRNAs indeed reduced expression of the 140-kD band and resulted in similar phenotypic changes as the original siRNAs that target all known Dbl isoforms (Fig. 1, D–F). Dbl3-depleted cells displayed reduced height (to ∼30%) and increased surface area (∼3.5-fold) and did not acquire the typical columnar cell shape (Fig. 1, F–J). Differentiated brush border membranes are enriched in F-actin. Dbl3 knockdown also resulted in cells with reduced integrated fluorescence density of stains for apical F-actin and DPPIV (Fig. 1, F, G, K, and L). Total DPPIV protein levels were unaffected (Fig. S2 B). In addition, depletion of the GEF also led to a diffuse distribution of the apical polarity regulator Crb3 without affecting its expression level (Fig. S2, C and D). Similarly, the brush border–associated ERM protein ezrin did not accumulate apically; its expression was not reduced and it was still found at cortex at the level of cell–cell contacts (Fig. S2, B and E). Dbl3 is thus required for epithelial columnar morphogenesis and apical differentiation.

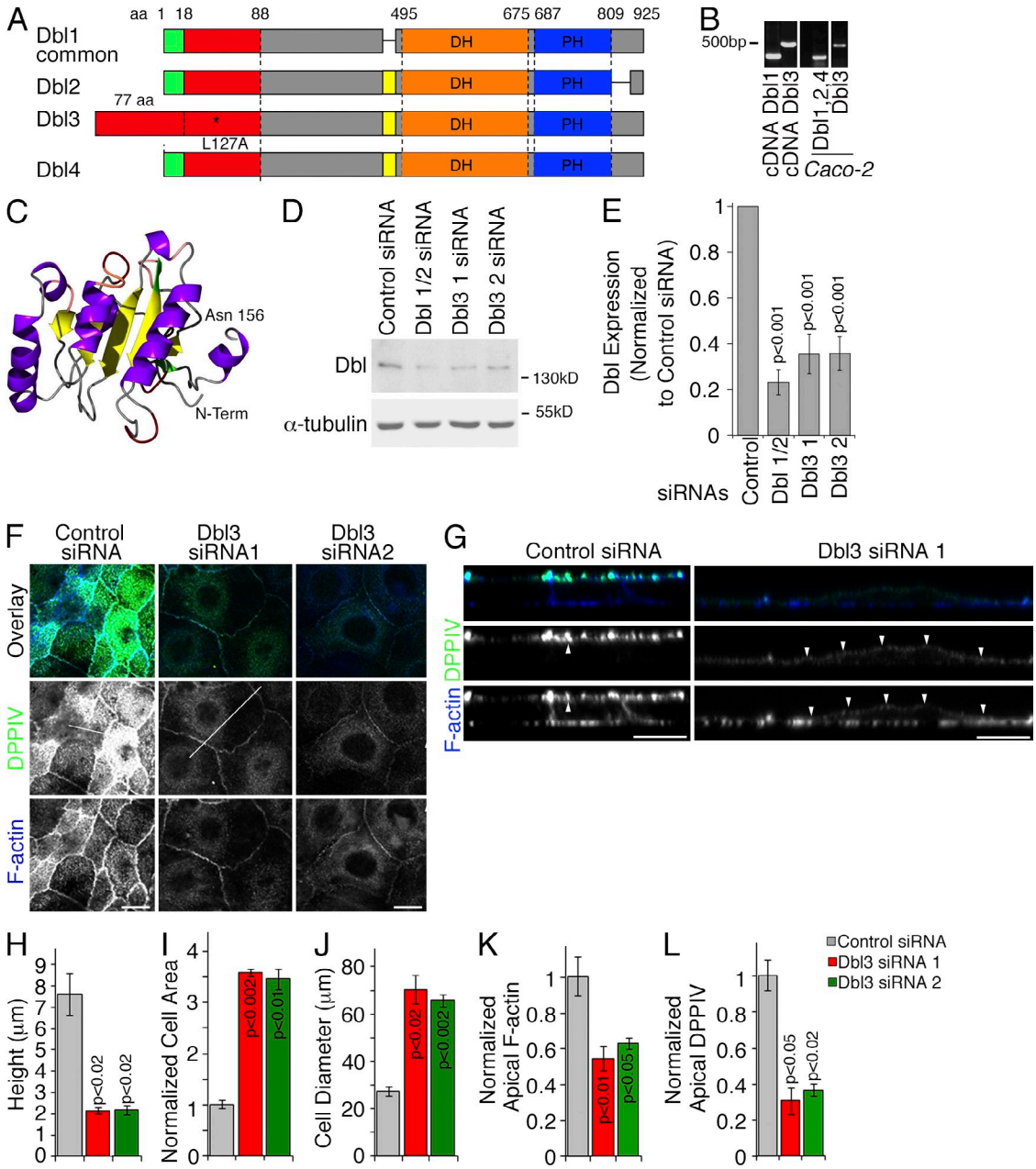


Figure 1. **Dbl3 regulates epithelial differentiation.** (A) Scheme of Dbl splice variants. The isoforms are numbered according to Komai et al. (2002). The commonly studied isoform and Dbl3 are also labeled. Note that DBL3 contains an intact Cral-Trio domain (indicated in red; L127A indicates a point mutation introduced to disrupt the domain). (B) mRNA expression of Dbl splice variants in Caco-2 cells. (C) Model of predicted structure of the Dbl3 N-terminal domain. Note that the N-terminal domains of the other isoforms do form Cral-Trio domains. (D–L) Caco-2 cells transfected with siRNAs were processed for immunoblotting (D and E) or immunofluorescence (F–L). (E) Quantification of Dbl depletion by densitometry (shown are means ± SD, $n = 4$; see Fig. S1 D for an example of a full-size blot). (F) Confocal xy sections taken from the apical end of the monolayers; the white lines indicate the positions at which the z line scans shown in G were taken (arrowheads point to the apical membrane). (H–L) Quantifications showing means ± SD of three independent experiments. Cell height was measured in z sections; cell diameter was measured along the longest axis of apical xy sections taken from the apical end of the monolayers; cell area was also measured in apical xy sections, reflecting the planar area of the cells; apical F-actin and DPPIV labeling was determined by measuring the integrated density over the apical membrane areas in xy sections. Bars, 10 μm.

## Dbl3 is required for epithelial morphogenesis and differentiation in 3D cultures

Because Dbl3 was required for morphogenesis of monolayer cultures, we next asked whether it is also required for epithelial morphogenesis in 3D cultures in which epithelial cells form polarized cysts with a lumen that is surrounded by a single cell layer (Bryant and Mostov, 2008).

After depletion of Dbl3, cysts were still able to form, although their morphology was altered (Fig. 2). Dbl3-depleted cells still formed predominantly single-lumen cysts in agreement with previous work with MDCK cysts (Qin et al., 2010). However, the lumens were smaller and irregularly shaped, and the lumen walls contained segments that were unusually thick, leading to an increase in the mean wall thickness (Fig. 2 C). As in 2D, apical DPPIV was reduced upon Dbl3 depletion

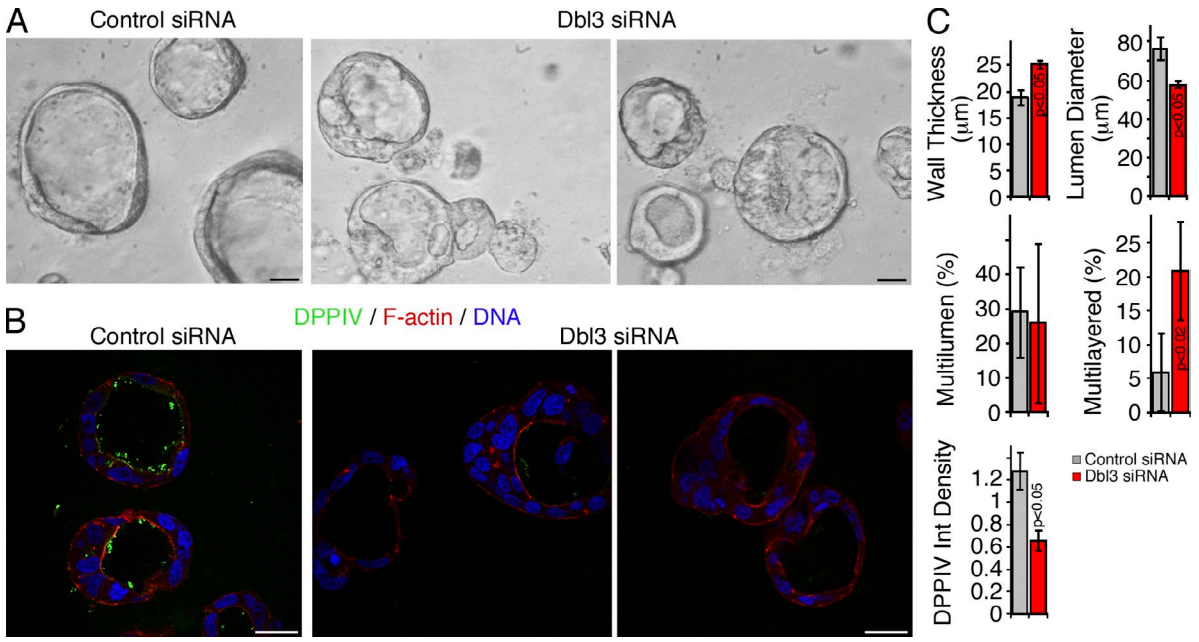


Figure 2. **Dbl3 is required for differentiation in epithelial 3D cultures.** Caco-2 cells were transfected with control and Dbl3 targeting siRNAs and were then cultured in 3D matrices before examination by phase contrast (A) and fixation followed by staining for the apical marker DPPIV, F-actin, and DNA (B). (C) Quantification of cyst morphology and expression of DPPIV. Wall thickness represents means of at least four measurements per cyst; the lumen diameter was determined along the longest axis of the cysts; the number of lumens and cysts with multilayered sections were determined by counting cysts in samples stained for DNA and F-actin; apical DPPIV labeling was assessed by measuring the integrated density. Shown are means ± SD of three independent experiments. Bars, 20 µm.

(Fig. 2, B and C). Staining of F-actin and nuclei revealed that the thick segments of the lumen wall were associated with areas not formed by a single layer of cells (Fig. 2, B and C). Dbl3 depletion thus leads to a defect in 3D epithelial morphogenesis.

### Dbl localizes to the apical membrane and is enriched at the apical margin

We next determined the localization of Dbl. In Caco-2 cells, anti-Dbl antibodies generated a punctate apical staining that was more enriched along cell–cell contacts and that was strongly reduced upon transfection of Dbl3 siRNAs (Fig. 3 A). By confocal microscopy, Dbl colocalized with ezrin, a protein that is essential for epithelial organization and apical membrane differentiation (Fig. 3 B; Saotome et al., 2004; Casaletto et al., 2011). Both proteins formed a more continuous pattern along the cell periphery (Fig. 3 B). Z sections revealed that Dbl and ezrin also localized throughout the apical brush border membrane (Fig. 3 C). Although the peripheral staining was reminiscent of tight junctions, Z sectioning revealed that Dbl did not precisely colocalize with ZO-1 but seemed to be positioned more apically (Fig. 3 D). Structured illumination super-resolution microscopy supported the enriched localization of Dbl and ezrin in a zone apical to the tight junction marker ZO-1, where they colocalized (Fig. 3, E and F). Ezrin-enriched brush border segments also revealed an overlapping distribution of Dbl and ezrin along the apical membrane and that the colocalization detected in confocal Z sections were often punctae of Dbl associated with ezrin-positive structures (Fig. 3 E).

Dbl is expressed in human and mouse epithelial tissues that form characteristically differentiated apical domains (Komai et al., 2002, 2003). Indeed, apical Dbl staining was observed in mouse tissue sections from the small intestine, colon, kidney, and retinal pigment epithelium (Fig. 3, G–J). Apical Dbl expression is thus a common feature of epithelia with morphologically characteristic apical membrane domains.

### The Carl-Trio domain is important for Dbl3 function

As Dbl3 is the only Dbl isoform with an intact Cral-Trio domain, we performed transient transfection experiments to test whether this domain affects Dbl-induced morphological responses. In addition to Caco-2 cells, we used MDCK cells, which, although polar, form a less distinctive apical membrane. The anti-Dbl antibodies also stained the apical membrane in MDCK cells, but the staining was weaker than in Caco-2 cells (Fig. S2 F). Expression of Dbl3 was also detected on the mRNA level, and the intensity of a band of 140 kD was reduced when MDCK cells were transfected with siRNAs targeting all Dbl isoforms or just Dbl3, indicating that MDCK cells also express Dbl3 (Fig. S2 G). We could not detect other Dbl isoforms in MDCK cells by RT-PCR. Both types of siRNAs reduced the levels of active Cdc42 in MDCK cells by ∼50% (Fig. S2 H).

In both cell lines, transfected Dbl3 localized apically and along cell–cell contacts, similar to the endogenous protein, and induced apically extended cells with more prominent apical F-actin staining, especially at cell–cell contacts between neighboring transfected cells (Fig. 4, A and B and Fig. S3, A and B). In contrast, transfected Dbl1 was distributed throughout the cytoplasm, and cells were spread across boundaries of neighboring cells in agreement with a previous study showing that

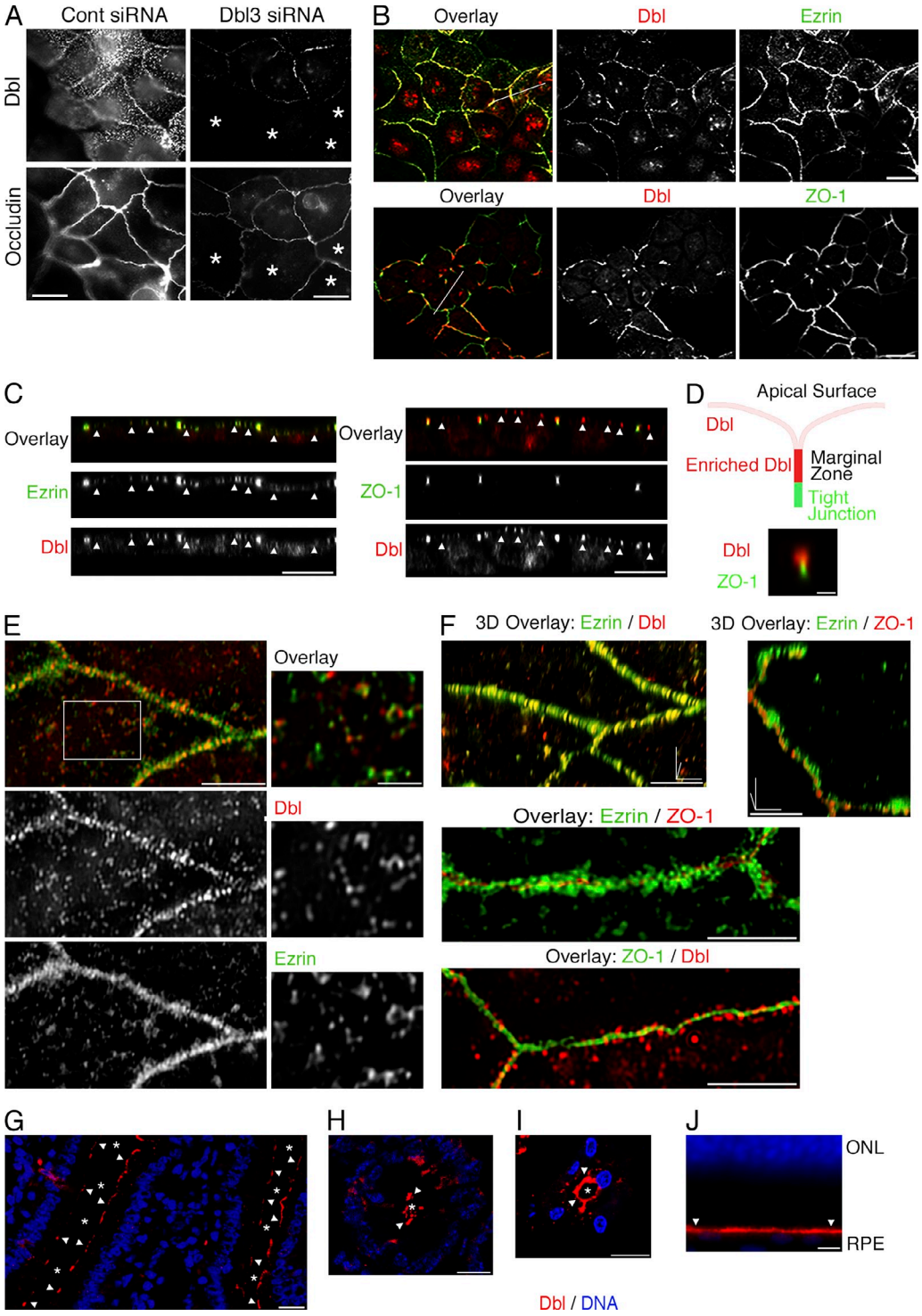


Figure 3. **Dbl associates with the apical membrane and is enriched in a marginal zone.** (A) Caco-2 cells transfected with siRNAs targeting Dbl3 were processed for immunofluorescence using antibodies against Dbl and occludin. Shown is an epifluorescence image of a field containing well and partially depleted cells. The asterisks mark cells that were well depleted. (B–F) Caco-2 cells were processed for immunofluorescence using antibodies against Dbl, ZO-1, and ezrin. The samples were then analyzed by confocal microscopy (B–D) or structured illumination super-resolution microscopy (G). (B) Single xy sections taken at the level of the apical junctional complex to determine the overlap between Dbl and ezrin with the junctional marker ZO-1. (C) Confocal z sections taken along the entire depth of the monolayers, and the arrowheads point to labeled apical membrane in images showing Dbl and ezrin. (E) A single structured illumination super-resolution microscopy image from the apical domain at which Dbl and ezrin are enriched; the box marks the position of the area that was enlarged and shows the association of Dbl- and ezrin-positive structures along the apical domain. (F) Single xy sections and 3D volume views generated from xy sections over an axial distance of 5 µm, which included the entire junctional complex to determine the relative localization of Dbl, ezrin, and ZO-1 at the apical–lateral border (indicated are the x, y, and z axes; the scale bar refers to the x axis). (G–J) Localization of Dbl in mouse intestine (G), colon (H), kidney (I), and retina (J). Arrowheads point to brush border membranes (G–I) and the apical membranes (J) of retinal pigment epithelial (RPE) cells (ONL, outer nuclear layer). The asterisks mark organ lumens. Bars: (A, C, and G–J) 10 µm; (B) 20 µm; (D) 1 µm; (E, left) 3 µm; (E, right) 1 µm; (F) 2 µm.

Dbl1 induces a transformed phenotype (Fig. S3, C and D; Prag et al., 2007). The main structural difference between Dbl3 and the other Dbl isoforms is the Cral-Trio domain. To test the importance of this domain, we substituted a leucine residue, L127, that is conserved in Cral-Trio domains (Table S1). Dbl3 carrying the L127A mutation no longer accumulated apically and at cell–cell contacts and did not induce apical F-actin reorganization (Fig. 4, A and B). Hence, an intact Cral-Trio domain is important for Dbl3 localization and function.

We next asked if the Cral-Trio domain is sufficient for apical targeting. A myc-tagged construct containing the Cral-Trio domain associated with the plasma as well as cytoplasmic membranes, indicating that the Cral-Trio domain on its own associates with membranes efficiently but nonspecifically (Fig. 4, C–E). Hence, an intact Cral-Trio domain is required for apical localization, but specific apical positioning requires additional structural elements.

### Ezrin mediates apical recruitment of Dbl3

As the Cral-Trio–like domain was not sufficient for specific apical recruitment, we asked what provides apical specificity. Dbl1 interacts with ezrin via its Pleckstrin homology domain, which is required for localization to the leading edge and is shared by all Dbl isoforms (Fig. 1 A; Vanni et al., 2004; Batchelor et al., 2007; Prag et al., 2007). Ezrin is a widely expressed apical scaffold protein and is important for apical differentiation (Berryman et al., 1993; Saotome et al., 2004; Fehon et al., 2010). As Dbl3 associates with apical ezrin-positive structures (Fig. 1), we tested whether ezrin is involved in its apical recruitment.

Depletion of ezrin led to phenotypic changes reminiscent of Dbl3 depletion, including flatter and more spread cells with poorly developed apical membranes (Fig. 5, A–H; and Fig. S3, E and F). It also resulted in loss of apical Dbl staining, suggesting that ezrin is required for Dbl3 recruitment (Fig. 5, I and J). As previously reported for Dbl1, ezrin coimmunoprecipitated with endogenous Dbl from Caco-2 and transfected Dbl3 from MDCK cells (Fig. 5 K). Expression of a hyperactive mutant form of ezrin (VSV-Ezrin T567D) resulted in increased apical recruitment, whereas expression of an inactive, dominant-negative form (VSV-N-ERMAD E244K) did not (Fig. 5, L and M). Ezrin thus forms complexes with Dbl3 and is required for its apical recruitment. Hence, apical enrichment of Dbl3 is based on two molecular mechanisms: binding to the apical scaffold ezrin, which interacts with the Pleckstrin homology domain of Dbl isoforms, and membrane binding by the Cral-Trio domain, which is unique to Dbl3.

### Dbl3 activates Cdc42 at apical cell–cell contacts

Dbl3 localizes to the apical membrane and is enriched at the apical margin close to the tight junction. Therefore, we asked whether Dbl3 regulates Cdc42 in a spatially controlled manner, using a fluorescence resonance energy transfer (FRET)-based active Cdc42 sensor that contains Cdc42 fused to the Cdc42/Rac interactive binding domain of PAK1 (Yoshizaki et al., 2003).

Cells transfected with nontargeting siRNAs exhibited the most intense FRET signal, indicating active Cdc42, along apical cell–cell contacts (Fig. 6, A and B; and Fig. S4 A). Depletion of Dbl with siRNAs against all isoforms or with siRNAs specifically targeting Dbl3 led to FRET signals that were lower and no longer concentrated at cell–cell contacts. Localization of GTP-bound Cdc42 using a specific antibody also revealed staining along apical cell–cell contacts that was sensitive to Dbl depletion (Fig. S4 B). Dbl3 is thus required for the normal levels of active Cdc42 at apical cell–cell contacts. Depletion of ezrin also led to a dispersed FRET signal, in agreement with ezrin's role in Dbl3 recruitment.

To determine the importance of the GEF activity, we generated tetracycline-inducible MDCK cells expressing either myc-tagged wild-type Dbl3 or a mutant carrying a point mutation in a tyrosine within a conserved QWIKKY motif (Dbl3-Y645A); analogous mutations in other Dbl family GEFs inactivate the exchange factor activity (Terry et al., 2011). Measurements of total GTP-Cdc42 levels confirmed that induction of myc-tagged Dbl3 stimulated Cdc42 activation, whereas Dbl3-Y645A did not (Fig. 6, C and D). Similarly, when these constructs were transfected into Caco-2 cells, wild-type Dbl3, but not the mutant, stimulated Cdc42 activation (Fig. S4 C). In agreement, staining with antibodies specific for GTP-bound Cdc42 demonstrated that active Cdc42 was induced at apical cell–cell contacts in cells expressing active but not mutant Dbl3 (Fig. 6 E), supporting the conclusion that Dbl3 functions as a GEF that stimulates spatially restricted activation of Cdc42 at apical cell–cell contacts.

As ezrin is required for Dbl3 recruitment, and both Dbl3 and ezrin depletion resulted in reduced apical Cdc42 activity, we tested whether enhanced ezrin function stimulates Cdc42 activation. Expression of active ezrin T567D, which stimulated enhanced Dbl recruitment (Fig. 5), resulted in a similar increase in active Cdc42 to expression of Dbl3-myc (Fig. 6, F and G). Combined expression of ezrin T567D and Dbl3-myc resulted in a further increase of active Cdc42 levels, supporting a model in which ezrin and Dbl3 cooperate in a pathway that promotes Cdc42 activation.

### Dbl3 regulates apical morphogenesis, domain size, and apical–lateral border position

The loss-of-function experiments indicate that Dbl3 regulates morphogenesis and apical differentiation. As MDCK cells have a poorly developed brush border membrane in comparison to Caco-2 cells, we next asked whether gain-of-function stimulates apical differentiation in MDCK cells. Phase-contrast microscopy revealed that expression of Dbl3 resulted in more compact cells with an apparently raised appearance (Fig. S5 A). Confocal microscopy showed that Dbl3 expression induced a strong increase in cell height, in the ezrin-positive membrane area, and integrated apical F-actin density; in contrast, α-catenin staining indicated a shortening of the lateral membrane (Fig. 7, A–C; and Fig. S5 B). All effects required an active GEF domain. The increase in ezrin-positive membrane area was not caused by higher expression levels (Fig. S5 C). Actin accumulation and apical expansion were prevented by depletion of ezrin, indicating that Dbl3's apical recruiter was required to induce the phenotype (Fig. 7, A and D; and Fig. S5, D and E).

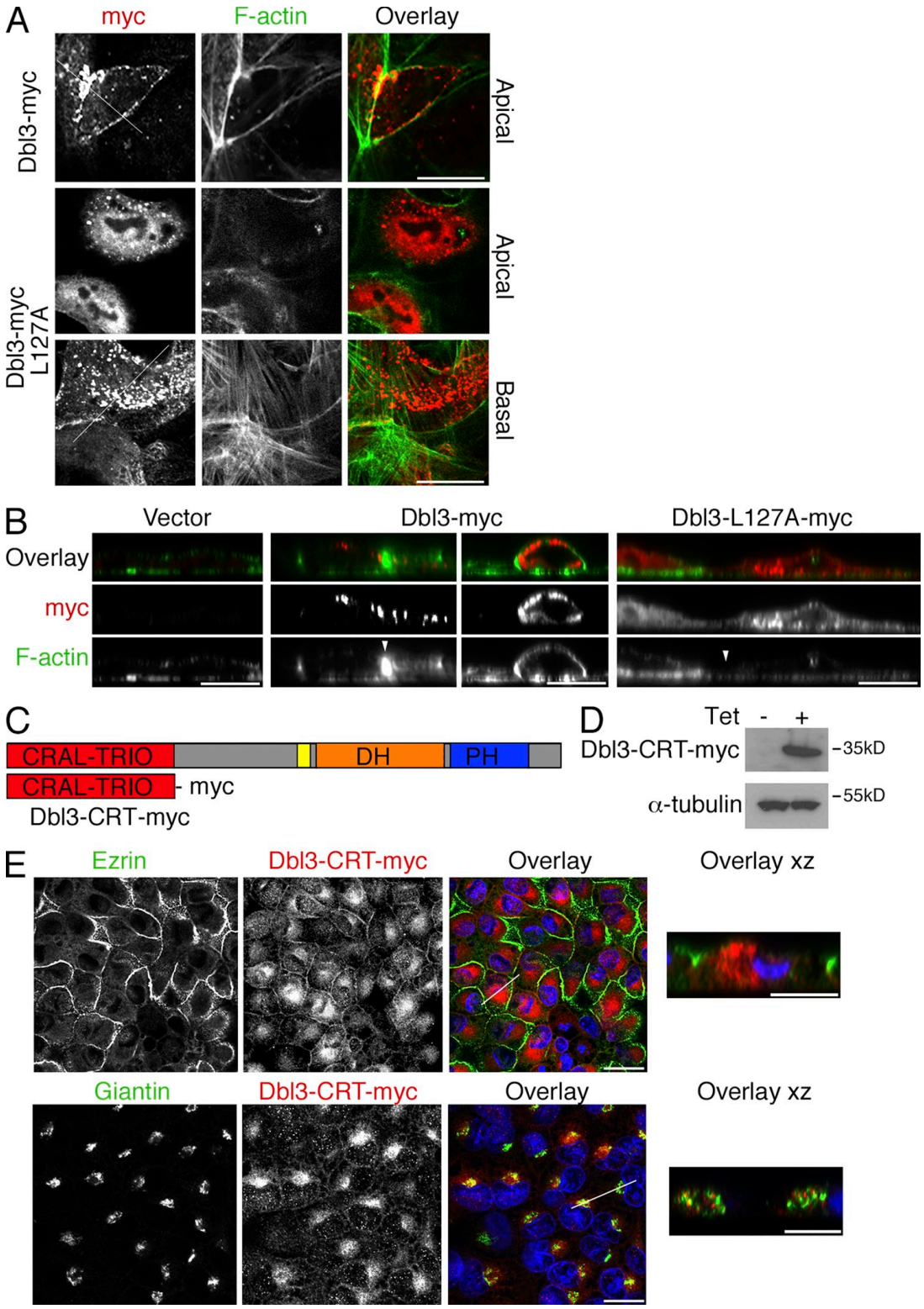


Figure 4. **The Cral-Trio domain is required for Dbl3 localization.** (A and B) Caco-2 cells were transiently transfected with myc-tagged cDNAs encoding wild-type Dbl3 or a mutant carrying a point mutation that substitutes a leucine residue that is conserved in Cral-Trio domains (see Table S1). Shown are confocal zy sections (A; white lines indicate position of z sections shown in B) and z sections (B; contacts between neighboring transfected cells are labeled with arrowheads). Two different images are shown for Dbl3-myc in B, illustrating the different effects observed in response to different expression levels. Note that wild-type Dbl3 is enriched along the apical membrane and cell–cell contacts and promotes enhanced F-actin staining at cell–cell contacts, whereas the mutant remains diffusely distributed in the cytoplasm and does not induced enhanced apical F-actin staining. See Fig. S3 (A–D) for expression of Dbl1 and localization of isoforms in MDCK cells. (C) Scheme of the Dbl3 domain structure and the CRAL-TRIO domain construct. (D and E) Dbl3-CRT-myc–expressing MDCK cells were processed for immunoblotting and immunofluorescence using antibodies against the proteins indicated. Bars: (A and B) 10 μm; (E, left) 20 μm; (E, right) 10 μm.

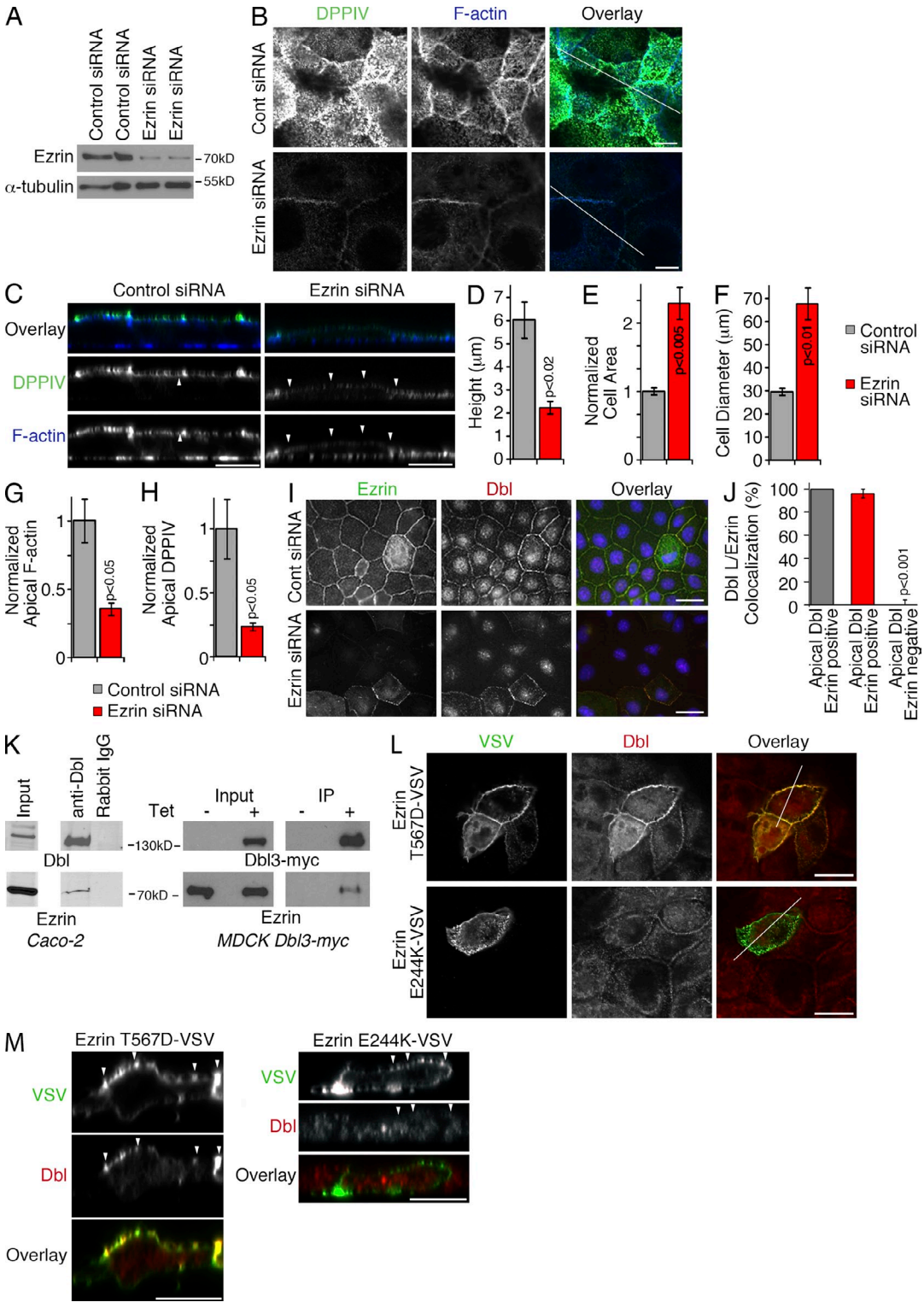


Figure 5. **Ezrin is required for apical recruitment of Dbl3.** (A–D) Caco-2 cells transfected with siRNAs were processed for immunoblotting (A) or immunofluorescence and confocal microscopy (B–H). The confocal images were then analyzed as described in Fig. 1. The quantification shows means ± SD of three independent experiments. The arrowheads in C point to the apical membrane. (I and J) Immunofluorescence analysis of Caco-2 cells transfected with siRNAs and labeled with antibodies against Dbl and Ezrin. (F) Cells still expressing detectable ezrin upon siRNA transfection were counted separately as an additional control (shown are means ± SD of three independent experiments). (K) Caco-2 or MDCK cells expressing Dbl3-myc in a tetracycline-regulated manner were processed for immunoprecipitation using anti-Dbl antibodies and were then blotted as indicated. (L and M) Caco-2 cells transiently transfected with Ezrin T567D-VSV or E244K-VSV cDNAs were analyzed by confocal microscopy (L, xy sections from the level of the apical–lateral border; M, z scans with arrowheads pointing to the apical membrane). Bars: (B, C, I, and M) 10 μm; (L) 20 μm.

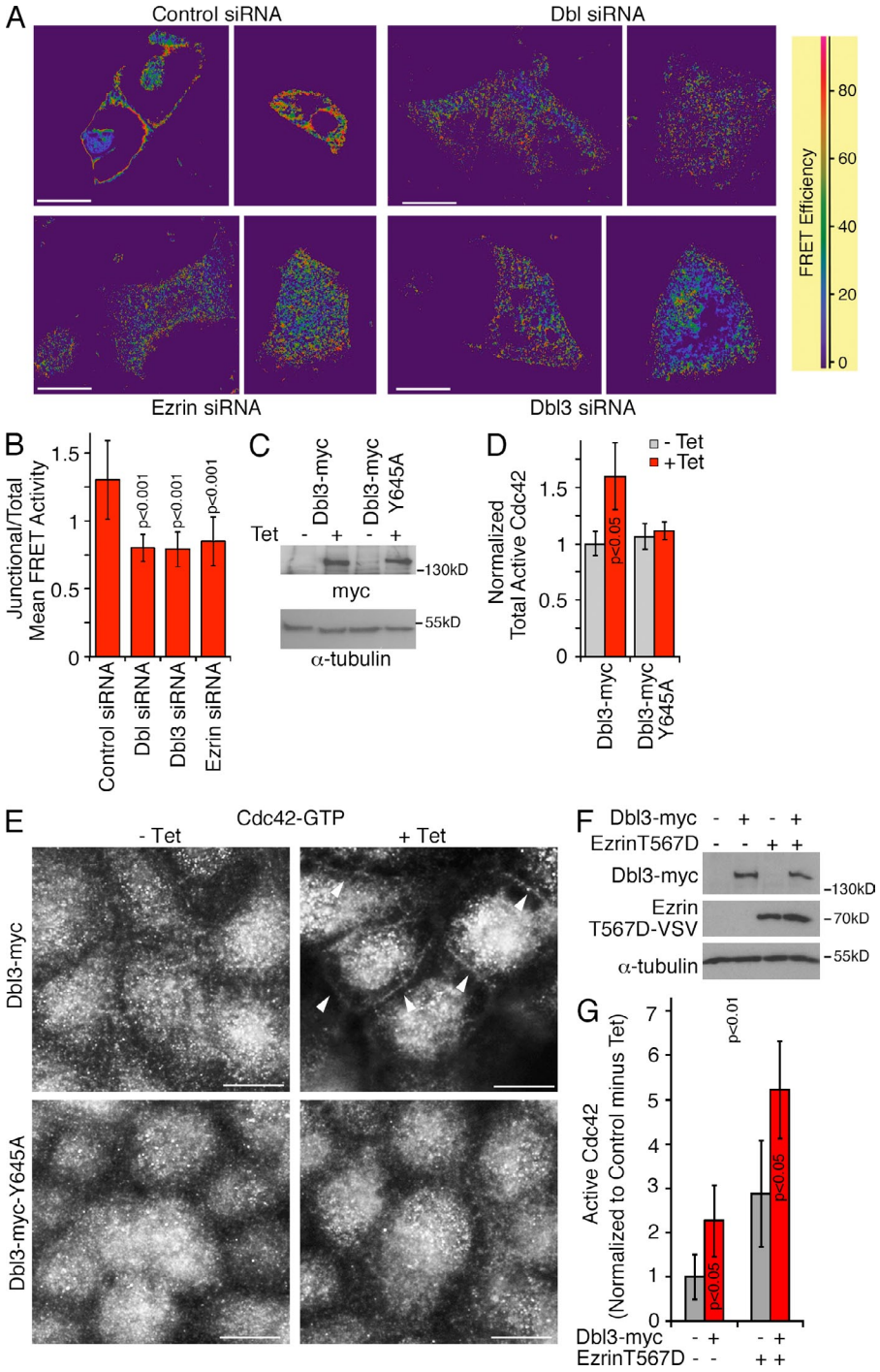


Figure 6. **Dbl3 drives polarized Cdc42 activation.** (A and B) Caco-2 monolayers transfected with siRNAs were analyzed for Cdc42 activity using a FRET biosensor. The images shown were taken from the apical area of the monolayers. High FRET activities reflect high Cdc42 activation levels. The quantification shows means ± SD ($n \geq 12$ imaged fields). See Fig. S4 A for absolute FRET efficiency values. (C and D) Tetracycline-inducible MDCK cell lines expressing myc-tagged wild type of GEF inactive Dbl3 were analyzed by immunoblotting (C) or for total active Cdc42 levels using the G-LISA assay (D; shown are means ± SD, $n = 3$). (E) The same MDCK cell lines were incubated with tetracycline for 4 h and processed for immunofluorescence using an antibody against Cdc42-GTP. Arrowheads point to cell–cell contacts. (F and G) MDCK cells were transfected with ezrinT567D-VSV without or with induction of Dbl3-myc expression. The cells were then analyzed by immunoblotting (F) or by measuring active Cdc42 levels using the G-LISA assay (G; shown are means ± SD, $n = 4$). Bars, 10 µm.

Expression of Dbl3 not only affected the distribution of ezrin and α-catenin but the tight junction marker ZO-1 localized closer to the basal membrane. It still bordered the apical ezrin staining, indicating that the apical–lateral border had shifted toward the basal membrane (Fig. 7 E). The apical polarity regulator Crb3 overlapped with ezrin, supporting an enhanced apical domain size (Fig. 7 F). Hence, expression of Dbl3 with an active GEF domain induced an increase in apical domain size and a shift of the apical–lateral border and cell junctions at the expense of the lateral membrane.

We next examined Dbl3-expressing MDCK cells using electron microscopy to determine if the observed apical expansion along the topologically lateral membrane was morphologically continuous. Analysis of ultrathin sections revealed that the apical membrane was morphologically extended and reached deep into lateral positions with no regularly apposed neighboring membranes, suggesting little cell–cell contact (Fig. 7 G). The nuclear positioning had become irregular, possibly caused by the compaction of the cells and their increased size. Scanning electron microscopy showed that control MDCK cells exhibited relatively few microvilli, which were not as regular as in in vivo; however, Dbl3-expressing cells exhibited an increase in microvilli-like projections (Fig. 7 H).

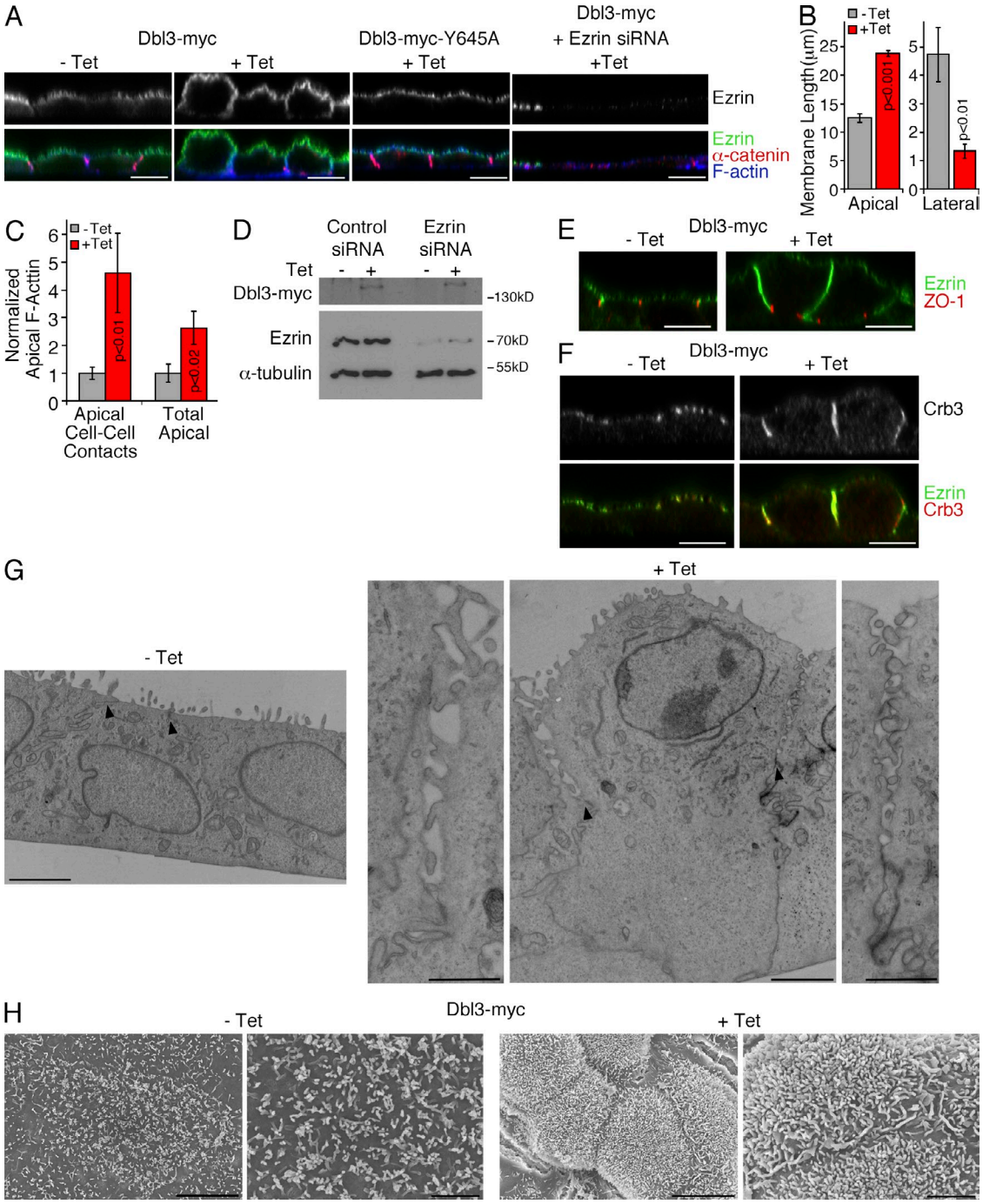


Figure 7. **Dbl3 regulates brush border induction and apical–lateral border positioning.** (A–C) MDCK cell lines induced with tetracycline for 8 h were analyzed by confocal z sectioning. If indicated, ezrin was depleted by siRNA transfection (see Fig. S5 for siRNA controls and xy images). Apical and lateral membrane lengths of Dbl3-Myc MDCK cells (B) and F-actin density of apical membrane at cell–cell contacts and total apical membrane (C) were measured before and after induction with tetracycline. (D) Dbl3-Myc MDCK cells were transfected with control or ezrin targeting siRNAs and were then incubated without or with tetracycline to induce induction of Dbl3 for 8 h before lysis and analysis by immunoblotting. (E and F) Dbl3-Myc MDCK cells were treated as in A before fixation and staining for the proteins indicated. Shown are confocal z sections. (G and H) Cells were processed for electron microscopy without or with induction of Dbl3-myc and analyzed by transmission (G) or scanning electron microscopy (H). Arrowheads indicate the position of tight junctions. Bars: (A, E, and F) 10 µm; (G, left) 1 µm; (G, right) 2 µm; (H, left) 2 µm; (H, right) 5 µm.

These data thus show that enhanced Dbl3 activity leads to an ezrin-dependent increase in apical domain size, enhanced apical features, and a shift of the apical–lateral border and tight junctions toward the basal membrane; hence, Dbl3 regulates the balance between apical and basolateral polarity factors in a pro-apical manner.

## Dbl3 is sufficient to stimulate morphogenesis and apical membrane differentiation

We next asked two questions. First, as Dbl3 is expressed in MDCK cells, does it possess a similar function to its role in Caco-2 cells. Second, as siRNAs specific for Dbl3 caused a

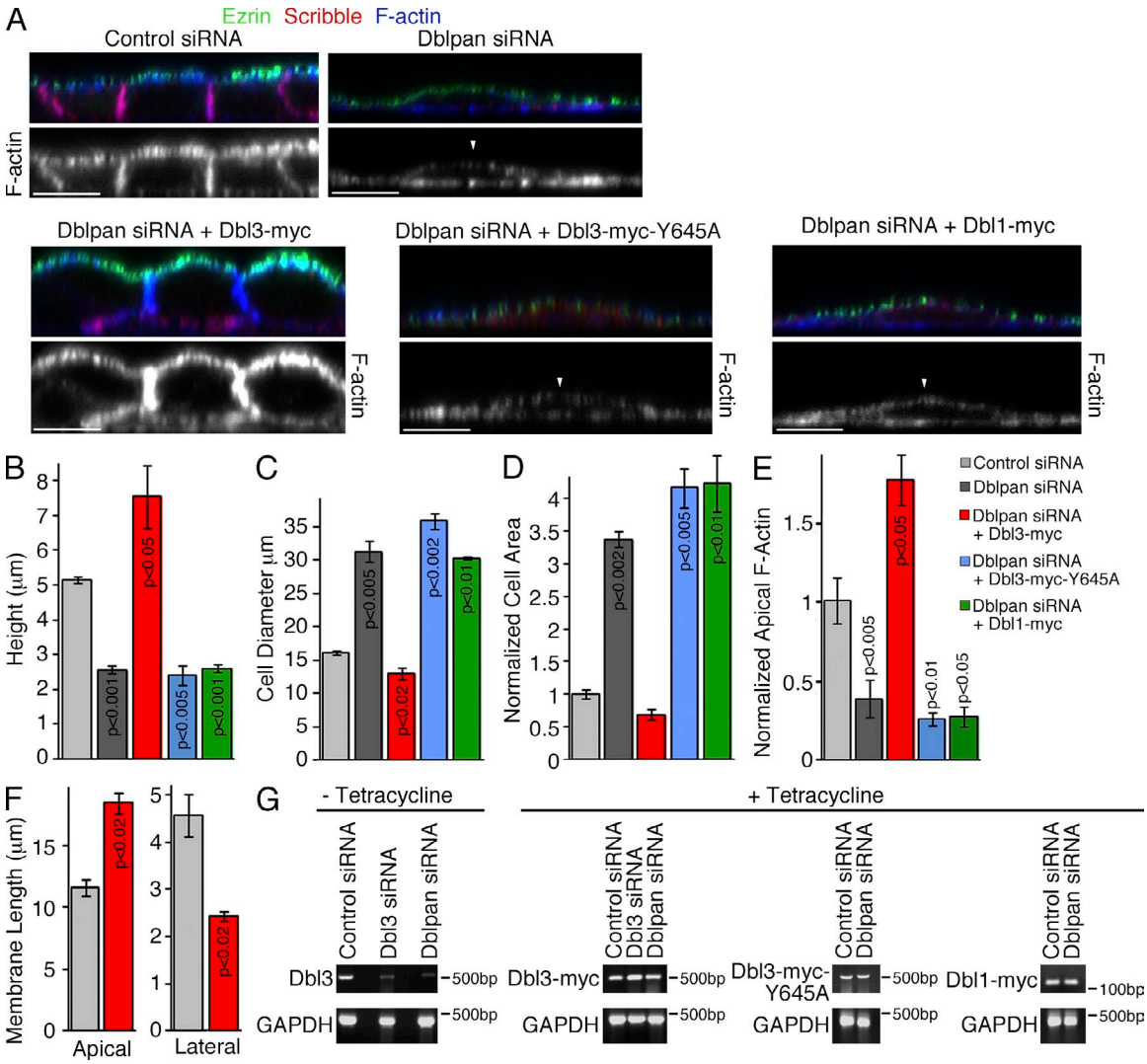


Figure 8. **Dbl3 is sufficient to stimulate morphogenesis and apical polarity.** MDCK cells were transfected with siRNAs and, if indicated, were induced to express wild-type or mutant Dbl isoforms for 8 h before fixation for immunofluorescence (A–F) or extraction of total RNA for RT-PCR (G). (A) Confocal z sections with arrowheads pointing to apical membranes. (B–F) Quantification showing means ± SD of three independent experiments, and all measurements were performed as in Fig. 1 (for B–E) and Fig. 7 (for F). Note that only expression of active Dbl3 can complement depletion of endogenous Dbl with siRNAs targeting all isoforms, and it recovers columnar morphogenesis as well as apical differentiation. Bars, 10 µm.

morphological defect in Caco-2 cells that was indistinguishable from siRNAs targeting all Dbl isoforms, is Dbl3 sufficient to induce epithelial differentiation? Depletion of Dbl in MDCK cells resulted in cells with similar phenotypic changes as in Caco-2: cells were reduced in height (~50%), cells were more spread (~3-fold), and the apical F-actin staining was reduced (~3-fold; Fig. 8 and Fig. S2, G and I). Dbl3 is thus required for columnar morphogenesis and apical differentiation of MDCK.

To determine whether Dbl3 is the only isoform required, we expressed human Dbl constructs in MDCK cells depleted with pan-Dbl siRNAs. Fig. 8 shows that Dbl3 was sufficient to stimulate cell compaction and apical differentiation independently, indicating that it is sufficient to drive epithelial differentiation. In contrast, stable expression of the Dbl1 did not rescue the defects caused by Dbl knockdown, supporting the different functional properties of Dbl isoforms. Expression of GEF-inactive Dbl3 (Dbl3-Y645A) also did not restore the phenotypic defects, supporting a specific role for Dbl3 in activating Cdc42 to drive epithelial differentiation.

These results thus demonstrate that Dbl3 is sufficient to drive cell compaction and columnerization, as well as apical extension and differentiation.

### Dbl3 drives the Par6–aPKC pathway

As Dbl3 determines positioning of the apical–lateral border, we asked whether this involved the Par3–Par6–aPKC pathway. Induction of Dbl3 expression in MDCK cells indeed stimulated enhanced accumulation of aPKCζ at cell–cell contacts and reduced cytoplasmic staining (Fig. 9 A). Staining for aPKCζ and Par6β extended along the lateral membrane until it reached the zone positive for scribble, marking shortened basolateral domains (Fig. 9, B–E). Par3, which remains associated with tight junctions upon junctional maturation, was also localized closer to the base of the cells (Fig. 9 B). Par3-positive foci were frequently

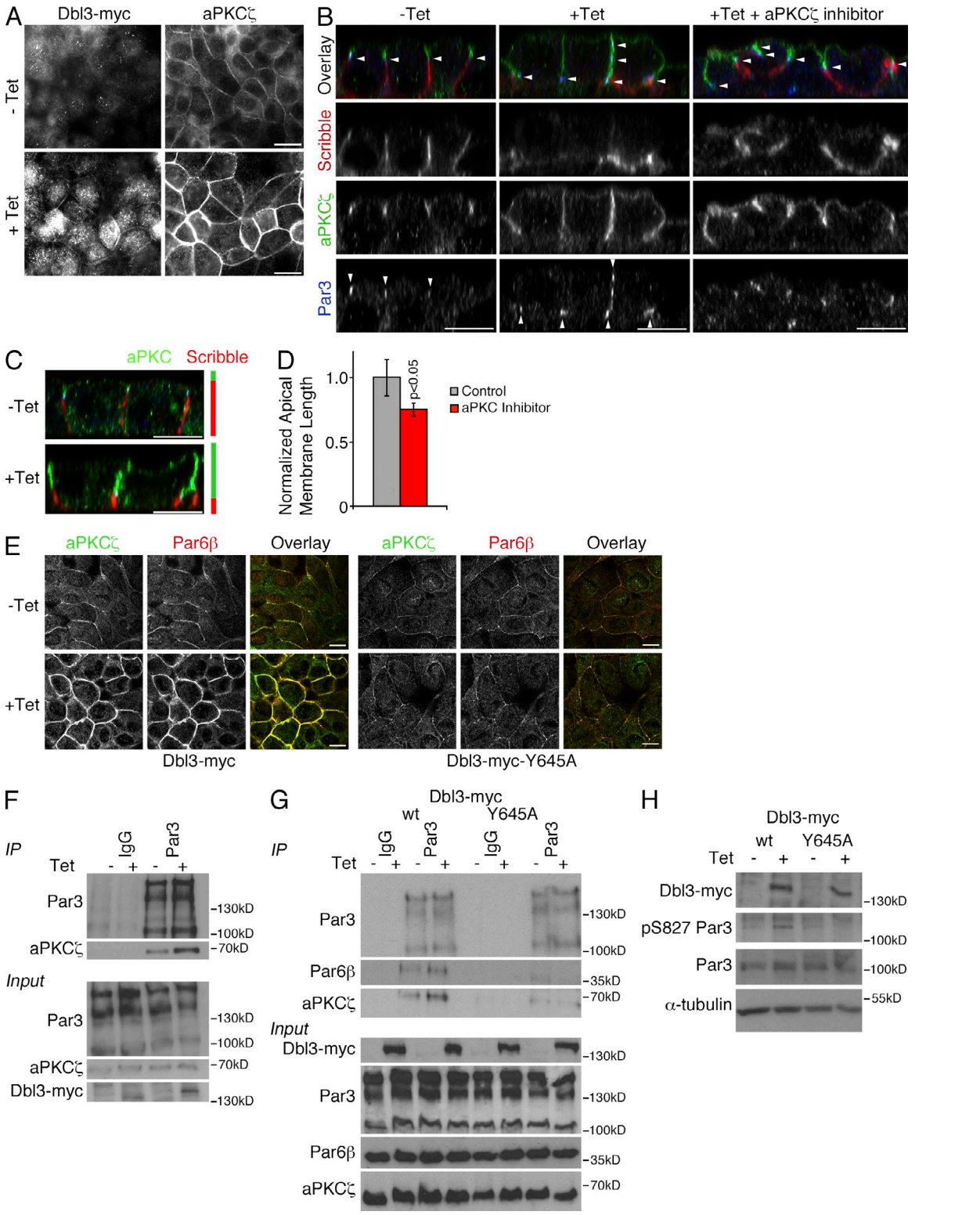


Figure 9. **Dbl3 controls progression of the Par3–Par6–aPKC pathway.** (A) Dbl3-myc MDCK cells induced with tetracycline for 4 h were stained with antibodies against Myc and aPKCζ. (B–D) Dbl3-myc MDCK cells were incubated with tetracycline for 8 h and, if indicated, aPKC inhibitor. The cells were then processed for immunofluorescence and analyzed by confocal microscopy. (C) The schematic indicates the relative distribution of the apical polarity regulator aPKC and the basolateral determinant scribble. (D) Quantification shows means ± SD of three independent experiments. (E) MDCK cells conditionally expressing Dbl3-myc or Dbl3-myc-Y645A were treated with tetracycline for 4 h and were then processed for immunofluorescence and confocal microscopy. Shown are confocal xy sections. Note, stimulation of aPKCζ and Par6β requires expression of active Dbl3. (F and G) Dbl3-myc MDCK cells were processed for immunoprecipitation using anti-Par3 or IgG control antibodies. Precipitates and lysates were then immunoblotted as indicated. (H) Induction of Par3 phosphorylation was analyzed by immunoblotting. Only one of the Par3 isoforms is shown as phosphorylation of the other ones was not detected. Bars, 10 µm.

observed along the lateral membrane and coincided with an incomplete lateral exclusion of scribble, indicating that the Dbl3 expression–stimulated repositioning of the apical–lateral border was still in progress as short induction times were analyzed.

Activation of the aPKC pathway in a dynamic system that is repositioning the apical–lateral border should lead to increased complex formation caused by the enhanced recruitment of aPKC but also increased phosphorylation of Par3, which promotes segregation of aPKC and Par6 into the increasing apical domain. Increased levels of coimmunoprecipitation of aPKCζ with Par3 in response to Dbl3 expression were indeed detected (Fig. 9 F). Increased complex formation was not induced when the GEF-inactive Dbl3-Y645A mutant was expressed (Fig. 9 G). Similar observations were made for Par6β (Fig. 9 G). Dbl3-induced Cdc42 activation thus stimulated formation of the transient tripartite complex.

Active aPKC phosphorylates serine-827 of Par3, which favors its dissociation and apical differentiation in *D. melanogaster* (Nagai-Tamai et al., 2002; Morais-de-Sá et al., 2010; Walther and Pichaud, 2010). Immunoblotting with an antibody specific for phosphorylated serine-827 indeed showed that induction of the active, but not mutant, Dbl3 stimulated phosphorylation of Par3 (Fig. 9 H). Inhibition of aPKC consequently attenuated the basal shift of the apical–lateral border and apical domain expansion (Fig. 9, B and D). Hence, aPKC activity was required for the Dbl3-driven expansion of the apical domain and basal shift of the apical–lateral border.

## Discussion

We have identified an activator of apically restricted and process-specific Cdc42 signaling. Dbl3 is a GEF that regulates epithelial morphogenesis, positioning of cell junctions, and the apical–lateral border, as well as apical domain differentiation and size. Dbl3 functions at a region above tight junctions, after their formation, promoting the progression of the Par3–Par6–aPKC pathway from junction formation to apical differentiation (Fig. 10).

Cdc42 regulates different processes required for epithelial differentiation (Hall, 2005). Hence, different GEFs and GAPs are required to control Cdc42 in space and time. Cdc42 regulators have been identified that regulate membrane traffic and junction assembly (Liu et al., 2004; Otani et al., 2006; Wells et al., 2006; Bryant et al., 2010; Elbediwy et al., 2012). However, the GEF that activates Cdc42 once junctions have been assembled to drive apical differentiation and apical–lateral border positioning by stimulating aPKC had thus far not been identified.

Dbl3 is recruited to the apical membrane in two steps: first, ezrin recruits the GEF to the apical domain and, second, the Cral-Trio domain then mediates stabilization at the membrane. Ezrin is required for epithelial organization and apical differentiation, and Dbl3 provides the molecular link between ezrin and apical Cdc42 signaling (Bonilha et al., 1999; Médina et al., 2002; Speck et al., 2003; Saotome et al., 2004; Cao et al., 2005; ten Klooster et al., 2009; Viswanatha et al., 2012). Although ezrin is required for apical targeting of Dbl3, isoform specificity is determined by the presence of a functional Cral-Trio domain. Cral-Trio domains can bind lipophilic molecules, which may

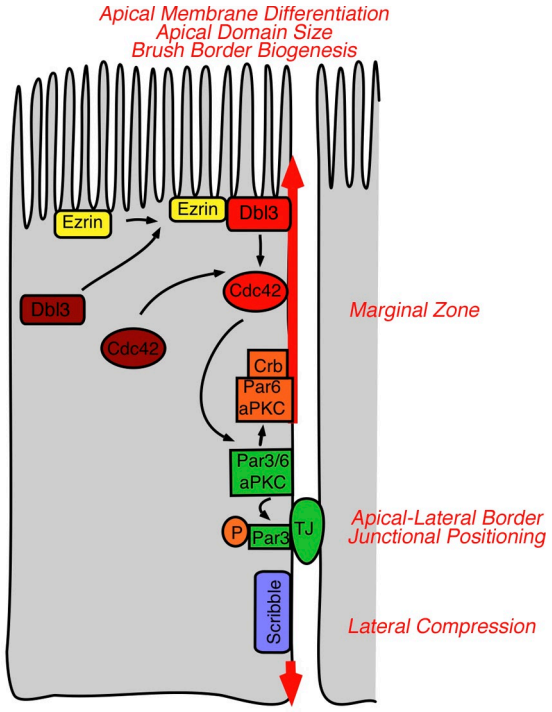


Figure 10. **Scheme of Dbl3 function.** A schematic drawing of an epithelial cell along with the processes regulated by Dbl3: apical differentiation, apical domain size, brush border biogenesis, apical lateral border positioning, and lateral compression. Labeled is also the vertebrate marginal zone immediately apical to the tight junction. Indicated is how Dbl3 is recruited to the apical membrane by ezrin where it becomes enriched at the marginal zone. Dbl3 then activates Cdc42, resulting in stimulation of the Par–Par6–aPKC pathway in a process-specific manner that leads to phosphorylation of Par3 and retention at tight junctions while Par6 and aPKC segregate into the expanding apical membrane.

be responsible for membrane recruitment (Panagabko et al., 2003). However, they do so in a promiscuous manner; hence, expression of the Cral-Trio domain alone resulted in nonspecific membrane recruitment. Thus, apical enrichment of Dbl3 requires the combination of ezrin-mediated targeting and Cral-Trio–mediated stabilization.

The interaction of Dbl3 with ezrin provides a direct link to the molecular network that regulates apical differentiation. Vertebrate ezrin and its fly counterpart bind to the apical crumbs complex by binding to the adaptor Pals1 or to crumbs itself (Médina et al., 2002; Speck et al., 2003; Cao et al., 2005). Ezrin is activated by phosphorylation by different kinases (ten Klooster et al., 2009; Viswanatha et al., 2012). One kinase, Mst4, functions downstream of the tumor suppressor Lkb1/Par4. Lkb1 may affect Dbl3 function, as the kinase can bind and stimulate the GEF activity of at least some Dbl isoforms (Xu et al., 2010). Similarly, the tumor suppressor hamartin/Tsc1 has been shown to bind and stimulate Dbl via the Dbl homology domain; the Tsc complex is regulated by the Crb3–PATJ complex (Massey-Harroche et al., 2007; Ognibene et al., 2011). Activation by tumor suppressors will thus be important to explore, as it may provide a molecular basis for the multilayering we observed in organotypic cultures of Dbl3-depleted cells. Dbl3 thus provides the missing molecular link between the ezrin–crumbs complex and the Cdc42-driven apical differentiation mechanisms,

as such a GEF had previously not been identified in any epithelial model system. Because Dbl3 is required for apical accumulation of Crb3, our results further suggest the existence of feedback mechanisms that enable the generation of a robust signal that drives apical differentiation.

The localization of Dbl3 suggests another evolutionarily conserved feature of the mechanisms that regulate apical differentiation. We observed that Ezrin and Dbl3 are enriched in a zone apical to tight junctions, the apical–lateral border in vertebrates, similar to a region in *D. melanogaster* termed the marginal zone that is also enriched in apical polarity regulators (Tepass, 2012). This domain became expanded when Dbl3 was expressed in MDCK cells. Therefore, our data suggest that the junctional configuration and the position of the apical signaling machinery relative to the apical–lateral border is evolutionarily conserved and that vertebrate epithelial cells also form an apical marginal zone in proximity to their apical–lateral border, the tight junction.

The molecular environment and spatial control of active Cdc42 is crucial for its function. Unlike increased Dbl3-mediated Cdc42 activity, increased Cdc42 signaling caused by depletion of the junction-associated Cdc42 GAPs did not lead to increased apical domain size but to defective junction assembly caused by diffusion of active Cdc42 (Wells et al., 2006; Elbediwy et al., 2012). Regulation of Cdc42 signaling during epithelial differentiation thus requires Cdc42 GEFs and GAPs that guide junction assembly, membrane traffic, and cytoskeletal organization, culminating with Dbl3 driving Cdc42 activation at an apical marginal zone to regulate apical differentiation and domain size and positioning of the apical–lateral border. Unlike Cdc42 GEFs that regulate junction formation, Dbl3 does not associate with the junctional complex but with the apical membrane and is enriched in a distinct zone apical to tight junctions. Thus, the recruitment of Dbl3 to the apical marginal zone ensures process-specific activation of Cdc42 and, hence, represents a functional barrier that separates junction formation from apical differentiation.

Activation of Cdc42 by Dbl3 leads to activation of the Par3–Par6–aPKC effector mechanism. This pathway regulates junction formation, apical differentiation, and junctional positioning (Suzuki and Ohno, 2006; Goldstein and Macara, 2007; Morais-de-Sá et al., 2010; Walther and Pichaud, 2010; St Johnston and Sanson, 2011). However, Dbl3 only stimulates the latter two functions. On a molecular level, this is supported by the observation that Dbl3 was required once the Par3–Par6–aPKC complex had been recruited to cell–cell contacts, a stage at which aPKC-mediated phosphorylation of Par3 promotes dissociation of the complex and enrichment of Par6–aPKC in the apical domain whereas Par3 remains associated with tight junctions. Hence, enhanced Dbl3 signaling led to increased recruitment of aPKC to the apical domain and increased phosphorylation of Par3.

Positioning of the apical–lateral border is a dynamic process and the underlying mechanism could be activated in already formed monolayers by overexpression of Dbl3. It is thus likely that the shift requires continuous turnover of tight junction complexes and of the machinery that determines apical–lateral border positioning. Such a dynamic model is supported by the observation that Dbl3-induced Cdc42 activation led to increased membrane recruitment of aPKC and increased coprecipitation of aPKC and Par6 with Par3 despite their increased accumulation in the apical, Par3-negative domain. Hence, apical–lateral border positioning seems to be mediated by a dynamic equilibrium between soluble and membrane-associated aPKC complexes, and forward flow of the pathway is driven by Dbl3-activated Cdc42 signaling. At least in MDCK cells, Dbl3 signaling seems to represent a rate-limiting step; hence, increased expression led to increased recruitment of aPKC and enhanced apical differentiation.

In conclusion, our data demonstrate that the differentiation of polarized epithelia culminates with the spatially restricted activation of Cdc42 by Dbl3 at a marginal apical zone located above tight junctions. Dbl3 is integrated into the evolutionarily conserved apical signaling machinery, functioning after initial junction formation, and drives apical membrane differentiation and size, morphological specialization (e.g., brush border membrane formation), and positioning of the apical–lateral border and tight junctions.

## Materials and methods

### Cell culture, cell lines, and permeability assays

Caco-2 and MDCK cells were cultured in high glucose DMEM containing 20% (Caco-2) or 10% (MDCK) heat-inactivated FCS with 100 µg/ml streptomycin and 100 µg/ml penicillin at 37°C in a 5% $CO_2$ atmosphere. Cells were cultured and plated for experiments as described previously (Matter et al., 1989; Steed et al., 2009). For calcium switch and permeability assays, cells transfected in 6-well plates were plated in low calcium medium containing dialyzed FCS (Elbediwy et al., 2012). Junction formation was then induced by adding normal tissue culture medium. For transepithelial electrical resistance and paracellular permeability assays, cells were cultured in 12-well culture inserts (0.4-µm pore size; Corning). Transepithelial electrical resistance was measured with a silver/silver-chloride electrode to determine the voltage deflection induced by an AC square wave current (±20 µA at 12.5 Hz) using an EVOM (World Precision Instruments, Inc.) as described previously (Matter and Balda, 2003). Paracellular permeability was determined over a time of 3 h after adding 4 kD of FITC-conjugated Dextran and 70 kD of Rhodamine B–conjugated dextran to the apical chamber, and a FLUOstar OPTIMA microplate reader (BMG LabTech) was then used to determine fluorescence in the basolateral chamber (Balda et al., 1996; Matter and Balda, 2003). The aPKCζ inhibitor (EMD Millipore) was used at a final concentration of 40 µM. For 3D cysts, siRNA-transfected Caco-2 cells were seeded on top of a layer of growth-factor reduced Matrigel 1 d after transfection (BD; Jaffe et al., 2008; Terry et al., 2011). In brief, coverslips in 48-well plates were covered with 120 µl Matrigel (9.8 mg/ml) and left to set for 1 h. 10,000 cells were then plated in 500 µl of low glucose medium containing 20% serum and 2% Matrigel. Cells were cultured for 3 d followed by the addition of 0.1 µg/ml cholera toxin and cultured for one further day before fixation.

### RNA interference, cDNAs, transfection, and RT-PCR

Full-length human Dbl isoform cDNAs (provided by S. Shiozawa; Kobe University, Kobe, Japan) were used to generate C-terminally myc-tagged constructs that were cloned into a pCDNA4/TO vector (Invitrogen). Point mutations L127A and Y645A were generated using the QuickChange mutagenesis kit (Agilent Technologies). Ezrin expression constructs were provided by T. Ng (King's College London, London, UK; Komai et al., 2002). The siRNA screen was performed as described previously (Elbediwy et al., 2012). In brief, Caco-2 cells were plated onto glass coverslips in 48-well plates and transfected the next day in triplicates with siRNAs from a library containing all known GEFs. After three days, the cells were fixed with and analyzed by immunofluorescence. In a first round, the cells were transfected with pools of siGenome siRNAs targeting four different sequences. Hits that affected either junction formation (based on ZO-1 distribution) or apical morphogenesis (based on DPPIV staining) were selected and

reanalyzed using pools of ON-TARGETplus siRNAs. Sequences targeted in the siRNA screen are provided in Table S2. siGenome and ON-TARGETplus siRNAs were obtained from Thermo Fisher Scientific, and custom siRNAs were obtained from Sigma-Aldrich. For subsequent RNAi experiments, cells were transfected with individual or pools of siRNAs targeting the following sequences: human Dbl, 5′-GCAACAGGAUCAAUUAACA-3′ and 5′-CUAGAAUGUCAUCGGCAAA-3′; human Dbl3, 5′-AAGACAUCGCCUUCUUGUCUU-3′ and 5′-AUACAUGGUCUUCUCUCAAUU-3′; canine Dbl, 5′-GCAACAGGAACUUAUGACA-3′ and 5′-CUUGAACACCACCACCAAA-3′; canine Dbl3, 5′-AAGAUAUCGCCUUCUUGUC-3′; human ezrin, 5′-GCGCGGAGCUGUCUAGUGA-3′ and 5′-GGAAUCAACUAUUUCGAGA-3′; and canine ezrin, 5′-GCGCUGAGCUGTCCAGCGA-3′ and 5′-GGAAUCAACUAUUUUGAGA-3′. For siRNA transfections, interferin transfection reagent (Polyplus-Transfection Inc.) was used according to the manufacturer's instructions using a total final siRNA concentration of 20–80 nM (Terry et al., 2011). Samples were collected and processed 3–4 d after transfection. For MDCK cells, siRNA-transfected cells were reseeded 1 d after transfection and cultured for 2–3 d followed by partial trypsinization and a second round of siRNA transfection. The cells were then harvested after a further 3–4 d. For DNA transfections, 0.5 µg/ml of plasmid DNA and JetPEI transfection reagent (Polyplus-Transfection Inc.) were used according to the manufacturer's instructions. Samples were collected and processed after 18–24 h. For the generation of tetracycline-regulated stable cell lines, MDCK cells were cotransfected with pcDNA6/TR and the respective Dbl3 expression vectors, and clones were subsequently selected as described previously (Aijaz et al., 2005; Terry et al., 2011). For RT-PCR, total RNA was isolated using the RNeasy kit (QIAGEN) and reverse transcribed with AMV reverse transcription before PCR (Nie et al., 2012). The following primers were used: human Dbl3, 5′-GGAAAGGACAATGCTTGGATC-3′ and 5′-CATCTGGTAGTTCTGTCTCAG-3′; human Dbl1, 5′-CCAATTTGTGGTACCCACACC-3′ and 5′-CTGACAATCAGGCACCACTTC-3′; human GAPDH, 5′-ATCACTGCCACCCAGAAGAC-3′ and 5′-ATGAGGTCCACCACCCTGTT-3′; canine GAPPDH, 5′-ATCACTGCCACCCAGAAGAC-3′ and 5′-ATGAGGTCCACCACCCGGTT-3′; canine Dbl3, 5′-GGAAAGGATAATGCTTGGATC-3′ and 5′-CATCTGGTAGTTCTGTCTCAG-3′; and canine Dbl1, 5′-CCAGTTTGTAGTGCCTGCTTC-3′ and 5′-CCGACAATCATGCACCACTTC-3′.

**Primary antibodies**

The following antibodies were used: rabbit anti-Dbl (sc-89) and Par6β, mouse anti-ezrin and aPKCζ, goat anti-scribble (Santa Cruz Biotechnology, Inc.); mouse anti–ZO-1 and anti-occludin (Invitrogen); rabbit anti-myc (MBL International); rabbit anti–α-catenin and β-catenin (Sigma-Aldrich); mouse anti–Cdc42-GTP (NewEast Biosciences); rabbit anti-Par3 (EMD Millipore); and mouse anti-p-MLC (S19; Cell Signaling Technology). The following antibodies were as described previously: rabbit anti-Crb3 (antigens: recombinant cytoplasmic domain of human Crb3 or the peptide N-VGARVPPTPNLKLPPEERLI-C; provided by B. Margolis [University of Michigan Medical School, Ann Arbor, MI] and A. Le Bivic [Developmental Biology Institute of Marseille Luminy, Marseille, France]), rabbit anti–ZO-1 (antigen: the peptide N-YTDQELDETLNDEVC-C), mouse anti–α-tubulin (antigen: a peptide containing the last 11 C-terminal amino acids of porcine α-tubulin), mouse anti-DPPIV (antigen: isolated human brush border membranes), mouse anti-Giantin (antigen: isolated Golgi membranes from Caco-2 cells), mouse and rabbit anti-VSV tag (antigen: the peptide N-CGYTDIEMNRLGK-C), and rabbit anti–phosphoS827-Par3 (antigen: the peptide N-CGFGRQS(P)MSEKR-C; provided by S. Ohno, Yokohama City University, Yokohama, Japan; Hauri et al., 1985; Kreis, 1986, 1987; Linstedt and Hauri, 1993; Nagai-Tamai et al., 2002; Benais-Pont et al., 2003; Makarova et al., 2003; Lemmers et al., 2004; Steed et al., 2009). A rabbit polyclonal antibody against human Dbl was raised against the peptide N-SSKQGKKTWRQNQSC-C and affinity purified using the peptide conjugated to Epoxy-activated Sepharose as described previously (Benais-Pont et al., 2003). This antibody was used for all experiments with human cells and for immunofluorescence in MDCK cells. The commercial anti-Dbl antibody was used for all other experiments.

**Immunostaining and fluorescence microscopy**

Cells were either fixed with methanol (5 min at −20°C) followed by rehydration in PBS at ambient temperature or with 3% PFA in PBS for 20 min at ambient temperature. PFA-fixed cells were then permeabilized with 0.3% Triton X-100 in PBS containing 0.5% BSA and 20 mM glycine for 3 min followed by two washes with blocking buffer (PBS with 0.5% BSA and 20 mM glycine; Balda et al., 1996). The samples were then incubated for 1 h in blocking buffer. After blocking and incubation with primary antibodies, which were diluted in blocking buffer, the samples were incubated with appropriate fluorescent cross-absorbed and affinity-purified secondary antibodies conjugated to Alexa 488, Cy3, Cy5, or Alexa 647 (Jackson ImmunoResearch Laboratories, Inc.) in blocking buffer. In some experiments, we used fluorescent phalloidin (Alexa 647; Molecular Probes) and Hoechst 33258 to label DNA (Invitrogen). 5-µm sections of mouse tissues were obtained and stained as described previously (Elbediwy et al., 2012; colon and small intestine sections were provided by P. Clark, Imperial College London, London, UK). All samples were embedded in ProLong Gold antifade reagent (Life Technologies). Epifluorescent images were collected with a DMIRB fluorescent microscope (Leica) using a Apochromat 63×/1.4 oil immersion objective fitted with a camera (C4742-95; Hamamatsu Photonics) and simple PCI software. Confocal images were acquired with an LSM 700 confocal laser scanning microscope (Leica) or an SP2 confocal microscope (Leica) using Apochromat 63×/1.4 immersion oil objectives. 518F immersion oil (Carl Zeiss) was used for all objectives. Images were acquired at ambient temperature using ZEN 2009 or Leica LCS, respectively. Images were adjusted for brightness and contrast with Adobe Photoshop. For FRET experiments, siRNA-transfected cells were plated into *ibidi* 8-well chamber slides and transfected with pRaichu-Cdc42 as previously described (Yoshizaki et al., 2003; Terry et al., 2011). The samples were analyzed using an SP2 microscope (Apochromat 63×/1.4 objective, 37°C) and LCS FRET software (Leica) using the donor recovery after acceptor bleaching protocol and generating the shown FRET efficiency maps according to the equation $[(D_{post} - D_{pre})/D_{post}] \times 100$ (D represents donor intensity). For quantification of relative FRET values, CFP images were subtracted and mean FRET intensities were quantified with ImageJ. For each image, all cell–cell contacts were quantified and normalizations were performed by dividing mean values obtained for specific fields by the mean values obtained for the entire field imaged (Elbediwy et al., 2012). For structured illumination super-resolution microscopy, the samples were prepared as for standard immunofluorescence using secondary antibody pairs conjugated to Alexa 488 and Cy3. The samples were then imaged with a microscope (N-SIM; Nikon) using the 3D-SIM mode and an Apochromat 60×/1.2 lens. The Nikon software was used for 3D reconstructions and brightness adjustments. Images were quantified using the measurement tools in Adobe Photoshop and ImageJ. For the analysis of single cells, at least 50 cells were analyzed for each condition in each experiment. Cell height was measured at at least four sites per cell that were placed at regular intervals along the entire width of the cells, and the mean value was then calculated for each cell. Similarly, cell diameters were measured parallel to the longest axis at at least four sites and averaged for each cell analyzed. Planar cell areas (e.g., the area covered in xy planes) were measured at the level of the apical junctional complex by tracing the cell perimeter. To quantify the fluorescence intensity (e.g., F-actin and DPPIV), the relevant areas (e.g., the apical membrane) were traced and the integrated density was calculated.

**Electron microscopy**

All steps were performed at room temperature with a rotator used during alcohol dehydration. Cell monolayers were fixed in a mixture of 3% (vol/vol) glutaraldehyde and 1% (wt/vol) PFA in 0.08 M sodium cacodylate buffer (CB), pH 7.4, for 2 h at room temperature and left overnight at 4°C. Before osmication, the primary fixative solution was replaced by a 0.08 M cacodylate buffered solution of 2.5% glutaraldehyde and 0.5% (wt/vol) tannic acid. After two brief rinses in CB, specimens were osmicated for 2 h in 1% (wt/vol) aqueous osmium tetroxide, dehydrated by 10-min incubations in 50%, 70%, 90%, and three times 100% ethanol. At his point specimens destined for examination by scanning electron microscopy were passed through two 5-min changes of hexamethyldisilazane and air dried. Once dried, specimens were cut out, mounted, sputter coated with 1 nm of platinum using a CR 108 coater (Cressington Scientific), and examined in a Sigma Field Emission scanning electron microscope (Carl Zeiss) operating at 5 kV. Digital images were recorded using SmartSEM software (Carl Zeiss). For transmission electron microscopy, wells were given a fourth change of absolute methanol and were then completely filled with araldite resin and placed in a 60°C oven overnight to harden. Semithin sections (0.75 µm) for light microscopy and ultrathin sections (50–70 nm) for electron microscopy were cut from sawed out blocks with diamond knives (Diatome; Leica). Semithin sections were stained with 1% toluidine blue/borax mixture at 60°C and ultrathin sections were stained with Reynold's lead citrate. Stained ultrathin sections were examined in a transmission electron microscopy (1010; JEOL) operating at 80 kV and images were recorded using an Orius B digital camera and DigitalMicrograph (Gatan, Inc.).

**Immunoblotting, immunoprecipitations, and Rho GTPase activity assays**

Whole cell lysates were collected after washing with PBS by adding SDS-PAGE sample buffer and heating at 70°C for 10 min. Extracts were homogenized using a 23-gauge needle and samples were processed using

standard Western blotting techniques. For immunoprecipitations, either Caco-2 cells or MDCK tetracycline-inducible DBL3-Myc–expressing cells were harvested using extraction buffer (10 mM Hepes, pH 7.4, 150 mM NaCl, 1% Triton X-100, 0.5% sodium deoxycholate, and 0.2% sodium dodecylsulfate) plus a cocktail protease and phosphatase inhibitors (Terry et al., 2011) and homogenized. Cell extract was incubated with inactivated CNBr beads on ice for 30 min followed by incubation with immunobeads for 2 h. Bead/extracts were washed twice with PBS-TX (PBS with 0.5% Triton X-100) and then PBS and processed for blotting using sample buffer. To measure total levels of active Rho GTPases, cells were transfected with siRNAs in 12-well plates and, after 72 h, extracts were analyzed for levels of active Rho GTPases using the respective G-LISA assay kits and following the manufacturer's protocol (Cytoskeleton; Terry et al., 2011).

### Structural analysis

The N-terminal regions of Dbl isoforms were submitted to the BioSerf option of the Psipred server (Buchan et al., 2010). Only the Dbl3 isoform sequence came back with a certain hit. A model using PDB 3hx3 as the template was then completed using the Modeller interface (Eswar et al., 2006). A similar model was constructed using Chimera based on a structural superposition of five Cral-Trio domains and then aligning the DBL3 N terminus to these sequences and completing a Modeller run through the chimera interface using 2d4q as the template (Pettersen et al., 2004). The region convincingly modeled is the N-terminal domain containing the first 156 residues of Dbl3.

### Statistical analysis

Averages and standard deviations were calculated and provided in the graphs. If not indicated otherwise, they were calculated from three independent experiments. The unpaired, two-tailed Student's *t* test was applied to calculate p-values.

### Online supplemental material

Fig. S1 shows the results of the siRNA screen for GEFs and the effect of Dbl depletion on tight junction function. Fig. S2 shows transfections of Dbl isoforms and their differential effect on cell morphology and the depletion of Dbl in MDCK cells. Fig. S3 shows the differential localization of transiently transfected Dbl isoforms and ezrin-dependent apical membrane formation. Fig. S4 shows localization of active Cdc42 in Caco-2 cells and how it is affected by Dbl depletion, and activation of Cdc42 in transfected Caco-2 cells. Fig. S5 shows the effect of active and inactive Dbl3 expression in MDCK cells on cell morphology and apical differentiation. Table S1 shows an alignment of Cral-Trio domains. Table S2 lists the sequences of the siRNAs used in the primary and secondary screens. Online supplemental material is available at http://www.jcb.org/cgi/content/full/jcb.201304064/DC1.

Ceniz Zihni wishes to dedicate this paper to his father, Mehmet Zihni, who passed away on the Nov. 21, 2012, while he was working on this project. You are my mentor of life and your love will always be my strength.

We are grateful to Shigeo Ohno, André Le Bivic, Ben Margolis, Tony Ng, Peter Clark, and Shunichi Shiozawa for providing valuable reagents.

This work was supported by the Wellcome Trust (084678/Z/08/Z and 099173/Z/12/Z) and the Biotechnology and Biological Sciences Research Council.

Submitted: 9 April 2013
Accepted: 25 November 2013

## References

Aijaz, S., F. D'Atri, S. Citi, M.S. Balda, and K. Matter. 2005. Binding of GEF-H1 to the tight junction-associated adaptor cingulin results in inhibition of Rho signaling and G1/S phase transition. *Dev. Cell*. 8:777–786. http://dx.doi.org/10.1016/j.devcel.2005.03.003

Balda, M.S., J.A. Whitney, C. Flores, S. González, M. Cereijido, and K. Matter. 1996. Functional dissociation of paracellular permeability and transepithelial electrical resistance and disruption of the apical-basolateral intramembrane diffusion barrier by expression of a mutant tight junction membrane protein. *J. Cell Biol.* 134:1031–1049. http://dx.doi.org/10.1083/jcb.134.4.1031

Batchelor, C.L., J.R. Higginson, Y.J. Chen, C. Vanni, A. Eva, and S.J. Winder. 2007. Recruitment of Dbl by ezrin and dystroglycan drives membrane proximal Cdc42 activation and filopodia formation. *Cell Cycle*. 6:353–363. http://dx.doi.org/10.4161/cc.6.3.3819

Benais-Pont, G., A. Punn, C. Flores-Maldonado, J. Eckert, G. Raposo, T.P. Fleming, M. Cereijido, M.S. Balda, and K. Matter. 2003. Identification of a tight junction-associated guanine nucleotide exchange factor that activates Rho and regulates paracellular permeability. *J. Cell Biol.* 160:729–740. http://dx.doi.org/10.1083/jcb.200211047

Berryman, M., Z. Franck, and A. Bretscher. 1993. Ezrin is concentrated in the apical microvilli of a wide variety of epithelial cells whereas moesin is found primarily in endothelial cells. *J. Cell Sci.* 105:1025–1043.

Bonilha, V.L., S.C. Finnemann, and E. Rodriguez-Boulan. 1999. Ezrin promotes morphogenesis of apical microvilli and basal infoldings in retinal pigment epithelium. *J. Cell Biol.* 147:1533–1548. http://dx.doi.org/10.1083/jcb.147.7.1533

Bryant, D.M., and K.E. Mostov. 2008. From cells to organs: building polarized tissue. *Nat. Rev. Mol. Cell Biol.* 9:887–901. http://dx.doi.org/10.1038/nrm2523

Bryant, D.M., A. Datta, A.E. Rodríguez-Fraticelli, J. Peränen, F. Martín-Belmonte, and K.E. Mostov. 2010. A molecular network for de novo generation of the apical surface and lumen. *Nat. Cell Biol.* 12:1035–1045. http://dx.doi.org/10.1038/ncb2106

Buchan, D.W., S.M. Ward, A.E. Lobley, T.C. Nugent, K. Bryson, and D.T. Jones. 2010. Protein annotation and modelling servers at University College London. *Nucleic Acids Res.* 38(Web Server issue):W563–W568.

Cao, X., X. Ding, Z. Guo, R. Zhou, F. Wang, F. Long, F. Wu, F. Bi, Q. Wang, D. Fan, et al. 2005. PALS1 specifies the localization of ezrin to the apical membrane of gastric parietal cells. *J. Biol. Chem.* 280:13584–13592. http://dx.doi.org/10.1074/jbc.M411941200

Casaletto, J.B., I. Saotome, M. Curto, and A.I. McClatchey. 2011. Ezrin-mediated apical integrity is required for intestinal homeostasis. *Proc. Natl. Acad. Sci. USA*. 108:11924–11929. http://dx.doi.org/10.1073/pnas.1103418108

Elbediwy, A., C. Zihni, S.J. Terry, P. Clark, K. Matter, and M.S. Balda. 2012. Epithelial junction formation requires confinement of Cdc42 activity by a novel SH3BP1 complex. *J. Cell Biol.* 198:677–693. http://dx.doi.org/10.1083/jcb.201202094

Eswar, N., B. Webb, M.A. Marti-Renom, M.S. Madhusudhan, D. Eramian, M.Y. Shen, U. Pieper, and A. Sali. 2006. Comparative protein structure modeling using Modeller. *Curr. Protoc. Bioinformatics*. 15:5.6.1–5.6.30.

Fehon, R.G., A.I. McClatchey, and A. Bretscher. 2010. Organizing the cell cortex: the role of ERM proteins. *Nat. Rev. Mol. Cell Biol.* 11:276–287. http://dx.doi.org/10.1038/nrm2866

Goldstein, B., and I.G. Macara. 2007. The PAR proteins: fundamental players in animal cell polarization. *Dev. Cell*. 13:609–622. http://dx.doi.org/10.1016/j.devcel.2007.10.007

Hall, A. 2005. Rho GTPases and the control of cell behaviour. *Biochem. Soc. Trans.* 33:891–895. http://dx.doi.org/10.1042/BST20050891

Hart, M.J., A. Eva, T. Evans, S.A. Aaronson, and R.A. Cerione. 1991. Catalysis of guanine nucleotide exchange on the CDC42Hs protein by the dbl oncogene product. *Nature*. 354:311–314. http://dx.doi.org/10.1038/354311a0

Hauri, H.-P., E.E. Sterchi, D. Bienz, J.A.M. Fransen, and A. Marxer. 1985. Expression and intracellular transport of microvillus membrane hydrolases in human intestinal epithelial cells. *J. Cell Biol.* 101:838–851. http://dx.doi.org/10.1083/jcb.101.3.838

Jaffe, A.B., N. Kaji, J. Durgan, and A. Hall. 2008. Cdc42 controls spindle orientation to position the apical surface during epithelial morphogenesis. *J. Cell Biol.* 183:625–633. http://dx.doi.org/10.1083/jcb.200807121

Kamynina, E., K. Kauppinen, F. Duan, N. Muakkassa, and D. Manor. 2007. Regulation of proto-oncogenic dbl by chaperone-controlled, ubiquitin-mediated degradation. *Mol. Cell. Biol.* 27:1809–1822. http://dx.doi.org/10.1128/MCB.01051-06

Komai, K., R. Okayama, M. Kitagawa, H. Yagi, K. Chihara, and S. Shiozawa. 2002. Alternative splicing variants of the human DBL (MCF-2) proto-oncogene. *Biochem. Biophys. Res. Commun.* 299:455–458. http://dx.doi.org/10.1016/S0006-291X(02)02645-1

Komai, K., N. Mukae-Sakairi, M. Kitagawa, and S. Shiozawa. 2003. Characterization of novel splicing variants of the mouse MCF-2 (DBL) proto-oncogene. *Biochem. Biophys. Res. Commun.* 309:906–909. http://dx.doi.org/10.1016/j.bbrc.2003.08.088

Kreis, T.E. 1986. Microinjected antibodies against the cytoplasmic domain of vesicular stomatitis virus glycoprotein block its transport to the cell surface. *EMBO J.* 5:931–941.

Kreis, T.E. 1987. Microtubules containing detyrosinated tubulin are less dynamic. *EMBO J.* 6:2597–2606.

Lemmers, C., D. Michel, L. Lane-Guermonprez, M.H. Delgrossi, E. Médina, J.P. Arsanto, and A. Le Bivic. 2004. CRB3 binds directly to Par6 and regulates the morphogenesis of the tight junctions in mammalian epithelial cells. *Mol. Biol. Cell*. 15:1324–1333. http://dx.doi.org/10.1091/mbc.E03-04-0235

Linstedt, A.D., and H.P. Hauri. 1993. Giantin, a novel conserved Golgi membrane protein containing a cytoplasmic domain of at least 350 kDa. *Mol. Biol. Cell*. 4:679–693. http://dx.doi.org/10.1091/mbc.4.7.679

Liu, X.F., H. Ishida, R. Raziuddin, and T. Miki. 2004. Nucleotide exchange factor ECT2 interacts with the polarity protein complex Par6/Par3/protein kinase Czeta (PKCzeta) and regulates PKCzeta activity. *Mol. Cell. Biol.* 24:6665–6675. http://dx.doi.org/10.1128/MCB.24.15.6665-6675.2004

Makarova, O., M.H. Roh, C.-J. Liu, S. Laurinec, and B. Margolis. 2003. Mammalian Crumbs3 is a small transmembrane protein linked to protein associated with Lin-7 (Pals1). *Gene*. 302:21–29. http://dx.doi.org/10.1016/S0378111902010843

Massey-Harroche, D., M.H. Delgrossi, L. Lane-Guermonprez, J.P. Arsanto, J.P. Borg, M. Billaud, and A. Le Bivic. 2007. Evidence for a molecular link between the tuberous sclerosis complex and the Crumbs complex. *Hum. Mol. Genet.* 16:529–536. http://dx.doi.org/10.1093/hmg/ddl485

Matter, K., and M.S. Balda. 2003. Functional analysis of tight junctions. *Methods*. 30:228–234. http://dx.doi.org/10.1016/S1046-2023(03)00029-X

Matter, K., W. McDowell, R.T. Schwartz, and H.P. Hauri. 1989. Asynchronous transport to the cell surface of intestinal brush border hydrolases is not due to differential trimming of N-linked oligosaccharides. *J. Biol. Chem.* 264:13131–13139.

Médina, E., J. Williams, E. Klipfell, D. Zarnescu, G. Thomas, and A. Le Bivic. 2002. Crumbs interacts with moesin and $\beta_{Heavy}$-spectrin in the apical membrane skeleton of *Drosophila*. *J. Cell Biol.* 158:941–951. http://dx.doi.org/10.1083/jcb.200203080

Mellman, I., and W.J. Nelson. 2008. Coordinated protein sorting, targeting and distribution in polarized cells. *Nat. Rev. Mol. Cell Biol.* 9:833–845. http://dx.doi.org/10.1038/nrm2525

Morais-de-Sá, E., V. Mirouse, and D. St Johnston. 2010. aPKC phosphorylation of Bazooka defines the apical/lateral border in *Drosophila* epithelial cells. *Cell*. 141:509–523. http://dx.doi.org/10.1016/j.cell.2010.02.040

Nagai-Tamai, Y., K. Mizuno, T. Hirose, A. Suzuki, and S. Ohno. 2002. Regulated protein-protein interaction between aPKC and PAR-3 plays an essential role in the polarization of epithelial cells. *Genes Cells*. 7:1161–1171. http://dx.doi.org/10.1046/j.1365-2443.2002.00590.x

Nie, M., M.S. Balda, and K. Matter. 2012. Stress- and Rho-activated ZO-1-associated nucleic acid binding protein binding to p21 mRNA mediates stabilization, translation, and cell survival. *Proc. Natl. Acad. Sci. USA*. 109:10897–10902. http://dx.doi.org/10.1073/pnas.1118822109

Ognibene, M., C. Vanni, D. Segalerba, P. Mancini, E. Merello, M.R. Torrisi, M.C. Bosco, L. Varesio, and A. Eva. 2011. The tumor suppressor hamartin enhances Dbl protein transforming activity through interaction with ezrin. *J. Biol. Chem.* 286:29973–29983. http://dx.doi.org/10.1074/jbc.M111.270785

Otani, T., T. Ichii, S. Aono, and M. Takeichi. 2006. Cdc42 GEF Tuba regulates the junctional configuration of simple epithelial cells. *J. Cell Biol.* 175:135–146. http://dx.doi.org/10.1083/jcb.200605012

Panagabko, C., S. Morley, M. Hernandez, P. Cassolato, H. Gordon, R. Parsons, D. Manor, and J. Atkinson. 2003. Ligand specificity in the CRAL-TRIO protein family. *Biochemistry*. 42:6467–6474. http://dx.doi.org/10.1021/bi034086v

Pettersen, E.F., T.D. Goddard, C.C. Huang, G.S. Couch, D.M. Greenblatt, E.C. Meng, and T.E. Ferrin. 2004. UCSF Chimera—a visualization system for exploratory research and analysis. *J. Comput. Chem.* 25:1605–1612. http://dx.doi.org/10.1002/jcc.20084

Pieczynski, J., and B. Margolis. 2011. Protein complexes that control renal epithelial polarity. *Am. J. Physiol. Renal Physiol.* 300:F589–F601. http://dx.doi.org/10.1152/ajprenal.00615.2010

Prag, S., M. Parsons, M.D. Keppler, S.M. Ameer-Beg, P. Barber, J. Hunt, A.J. Beavil, R. Calvert, M. Arpin, B. Vojnovic, and T. Ng. 2007. Activated ezrin promotes cell migration through recruitment of the GEF Dbl to lipid rafts and preferential downstream activation of Cdc42. *Mol. Biol. Cell*. 18:2935–2948. http://dx.doi.org/10.1091/mbc.E06-11-1031

Qin, Y., W.H. Meisen, Y. Hao, and I.G. Macara. 2010. Tuba, a Cdc42 GEF, is required for polarized spindle orientation during epithelial cyst formation. *J. Cell Biol.* 189:661–669. http://dx.doi.org/10.1083/jcb.201002097

Ratheesh, A., G.A. Gomez, R. Priya, S. Verma, E.M. Kovacs, K. Jiang, N.H. Brown, A. Akhmanova, S.J. Stehbens, and A.S. Yap. 2012. Centralspindlin and α-catenin regulate Rho signalling at the epithelial zonula adherens. *Nat. Cell Biol.* 14:818–828. http://dx.doi.org/10.1038/ncb2532

Saotome, I., M. Curto, and A.I. McClatchey. 2004. Ezrin is essential for epithelial organization and villus morphogenesis in the developing intestine. *Dev. Cell*. 6:855–864. http://dx.doi.org/10.1016/j.devcel.2004.05.007

Snyder, J.T., D.K. Worthylake, K.L. Rossman, L. Betts, W.M. Pruitt, D.P. Siderovski, C.J. Der, and J. Sondek. 2002. Structural basis for the selective activation of Rho GTPases by Dbl exchange factors. *Nat. Struct. Biol.* 9:468–475. http://dx.doi.org/10.1038/nsb796

Speck, O., S.C. Hughes, N.K. Noren, R.M. Kulikauskas, and R.G. Fehon. 2003. Moesin functions antagonistically to the Rho pathway to maintain epithelial integrity. *Nature*. 421:83–87. http://dx.doi.org/10.1038/nature01295

St Johnston, D., and B. Sanson. 2011. Epithelial polarity and morphogenesis. *Curr. Opin. Cell Biol.* 23:540–546. http://dx.doi.org/10.1016/j.ceb.2011.07.005

Steed, E., N.T. Rodrigues, M.S. Balda, and K. Matter. 2009. Identification of MarvelD3 as a tight junction-associated transmembrane protein of the occludin family. *BMC Cell Biol.* 10:95. http://dx.doi.org/10.1186/1471-2121-10-95

Suzuki, A., and S. Ohno. 2006. The PAR-aPKC system: lessons in polarity. *J. Cell Sci.* 119:979–987. http://dx.doi.org/10.1242/jcs.02898

ten Klooster, J.P., M. Jansen, J. Yuan, V. Oorschot, H. Begthel, V. Di Giacomo, F. Colland, J. de Koning, M.M. Maurice, P. Hornbeck, and H. Clevers. 2009. Mst4 and Ezrin induce brush borders downstream of the Lkb1/Strad/Mo25 polarization complex. *Dev. Cell*. 16:551–562. http://dx.doi.org/10.1016/j.devcel.2009.01.016

Tepass, U. 2012. The apical polarity protein network in *Drosophila* epithelial cells: regulation of polarity, junctions, morphogenesis, cell growth, and survival. *Annu. Rev. Cell Dev. Biol.* 28:655–685. http://dx.doi.org/10.1146/annurev-cellbio-092910-154033

Terry, S.J., C. Zihni, A. Elbediwy, E. Vitiello, I.V. Leefa Chong San, M.S. Balda, and K. Matter. 2011. Spatially restricted activation of RhoA signalling at epithelial junctions by p114RhoGEF drives junction formation and morphogenesis. *Nat. Cell Biol.* 13:159–166. http://dx.doi.org/10.1038/ncb2156

Vanni, C., A. Parodi, P. Mancini, V. Visco, C. Ottaviano, M.R. Torrisi, and A. Eva. 2004. Phosphorylation-independent membrane relocalization of ezrin following association with Dbl in vivo. *Oncogene*. 23:4098–4106. http://dx.doi.org/10.1038/sj.onc.1207509

Viswanatha, R., P.Y. Ohouo, M.B. Smolka, and A. Bretscher. 2012. Local phosphocycling mediated by LOK/SLK restricts ezrin function to the apical aspect of epithelial cells. *J. Cell Biol.* 199:969–984. http://dx.doi.org/10.1083/jcb.201207047

Walther, R.F., and F. Pichaud. 2010. Crumbs/DaPKC-dependent apical exclusion of Bazooka promotes photoreceptor polarity remodeling. *Curr. Biol.* 20:1065–1074. http://dx.doi.org/10.1016/j.cub.2010.04.049

Wells, C.D., J.P. Fawcett, A. Traweger, Y. Yamanaka, M. Goudreault, K. Elder, S. Kulkarni, G. Gish, C. Virag, C. Lim, et al. 2006. A Rich1/Amot complex regulates the Cdc42 GTPase and apical-polarity proteins in epithelial cells. *Cell*. 125:535–548. http://dx.doi.org/10.1016/j.cell.2006.02.045

Xu, X., T. Omelchenko, and A. Hall. 2010. LKB1 tumor suppressor protein regulates actin filament assembly through Rho and its exchange factor Dbl independently of kinase activity. *BMC Cell Biol.* 11:77. http://dx.doi.org/10.1186/1471-2121-11-77

Yamanaka, T., and S. Ohno. 2008. Role of Lgl/Dlg/Scribble in the regulation of epithelial junction, polarity and growth. *Front. Biosci.* 13:6693–6707. http://dx.doi.org/10.2741/3182

Yano, T., Y. Yamazaki, M. Adachi, K. Okawa, P. Fort, M. Uji, S. Tsukita, and S. Tsukita. 2011. Tara up-regulates E-cadherin transcription by binding to the Trio RhoGEF and inhibiting Rac signaling. *J. Cell Biol.* 193:319–332. http://dx.doi.org/10.1083/jcb.201009100

Yoshizaki, H., Y. Ohba, K. Kurokawa, R.E. Itoh, T. Nakamura, N. Mochizuki, K. Nagashima, and M. Matsuda. 2003. Activity of Rho-family GTPases during cell division as visualized with FRET-based probes. *J. Cell Biol.* 162:223–232. http://dx.doi.org/10.1083/jcb.200212049